ARTICLE   OPEN

Check for updates

Early activation of cellular stress and death pathways caused by cytoplasmic TDP-43 in the rNLS8 mouse model of ALS and FTD

Wei Luan[1], Amanda L. Wright[1,2], Heledd Brown-Wright[1], Sheng Le[2], Rebecca San Gil [1], Lidia Madrid San Martin[1], Karen Ling [3], Paymaan Jafar-Nejad[3], Frank Rigo[3] and Adam K. Walker [1,2✉]

TAR DNA binding protein 43 (TDP-43) pathology is a key feature of over 95% of amyotrophic lateral sclerosis (ALS) and nearly half of frontotemporal dementia (FTD) cases. The pathogenic mechanisms of TDP-43 dysfunction are poorly understood, however, activation of cell stress pathways may contribute to pathogenesis. We, therefore, sought to identify which cell stress components are critical for driving disease onset and neurodegeneration in ALS and FTD. We studied the rNLS8 transgenic mouse model, which expresses human TDP-43 with a genetically-ablated nuclear localisation sequence within neurons of the brain and spinal cord resulting in cytoplasmic TDP-43 pathology and progressive motor dysfunction. Amongst numerous cell stress-related biological pathways profiled using qPCR arrays, several critical integrated stress response (ISR) effectors, including CCAAT/enhancer-binding homologous protein (Chop/Ddit3) and activating transcription factor 4 (Atf4), were upregulated in the cortex of rNLS8 mice prior to disease onset. This was accompanied by early up-regulation of anti-apoptotic gene Bcl2 and diverse pro-apoptotic genes including BH3-interacting domain death agonist (Bid). However, pro-apoptotic signalling predominated after onset of motor phenotypes. Notably, pro-apoptotic cleaved caspase-3 protein was elevated in the cortex of rNLS8 mice at later disease stages, suggesting that downstream activation of apoptosis drives neurodegeneration following failure of early protective responses. Unexpectedly, suppression of Chop in the brain and spinal cord using antisense oligonucleotide-mediated silencing had no effect on overall TDP-43 pathology or disease phenotypes in rNLS8 mice. Cytoplasmic TDP-43 accumulation therefore causes very early activation of ISR and both anti- and pro-apoptotic signalling that switches to predominant pro-apoptotic activation later in disease. These findings suggest that precise temporal modulation of cell stress and death pathways may be beneficial to protect against neurodegeneration in ALS and FTD.

INTRODUCTION

Amyotrophic lateral sclerosis (ALS) and frontotemporal dementia (FTD) are neurodegenerative diseases that share multiple pathological features, particularly the presence of intracellular protein inclusions. Of proteins contributing to disease, ubiquitinated, phosphorylated, and biochemically-insoluble forms of TAR DNA binding protein 43 (TDP-43) lead to neurodegeneration in >95% of both sporadic and familial ALS cases and about 45% of FTD cases [1, 2]. TDP-43 is an important RNA-binding protein that typically shuttles between the nucleus and cytoplasm under physiological conditions, but TDP-43 accumulation in the cytoplasm of neurons results in neurodegeneration [3, 4]. The pathways leading to neuronal demise caused by cytoplasmic TDP-43 pathology remain to be fully defined [5], and understanding the mechanisms that cause neuron death may reveal new therapeutic opportunities.

Many pathogenic mechanisms have been proposed to contribute to neurodegeneration in ALS, including the integrated stress response (ISR) [6], protein synthesis dysregulation [7], oxidative stress [6], and neuroinflammation [8, 9]. Indeed, chronic activation of the ISR likely contributes to motor neuron death in

ALS and FTD [10, 11]. The ISR is a master regulatory pathway that fine-tunes proteostasis in cells, controlling protein synthesis, folding, and decay processes, and is crucial for cell survival [11]. Under diverse cellular stress conditions, ISR signaling upregulates select downstream transcripts to restore protein homeostasis. Activating transcription factor 4 (ATF4) is a crucial ISR regulator that targets genes to promote protein folding and degradation, increasing cell survival [12]. Nevertheless, prolonged disturbance of proteostasis enhances ISR signaling and consequently results in ATF4-mediated upregulation of CCAAT/enhancer-binding homologous protein (CHOP), which can trigger a pro-apoptotic signal cascade [11, 13]. ISR activation, evidenced by activation of ISR sensor kinases, has been reported in postmortem samples of ALS cases [6]. Moreover, activation of ISR enhances TDP-43 aggregation and stress granule formation, which are hallmarks of TDP-43-linked disease [14–16], suggesting a direct association of TDP-43 dysfunction with ISR activation. In addition, TDP-43 toxicity increases levels of CHOP protein in cell lines and sporadic ALS spinal cord tissues [15, 17]. Pharmacological modulation for ISR using small-molecule drugs can modify neurodegeneration [7], however, the actions of these drugs are not restricted to the ISR

[1]Neurodegeneration Pathobiology Laboratory, Queensland Brain Institute, University of Queensland, St Lucia, QLD, Australia. [2]Centre for Motor Neuron Disease Research, Macquarie Medical School, Macquarie University, Sydney, NSW, Australia. [3]Ionis Pharmaceuticals, Carlsbad, CA 90201, USA. ✉email: adam.walker@uq.edu.au

pathways. Therefore, it remains unclear whether specific modulation of ISR effectors can modulate disease in mammalian models of cytoplasmic TDP-43 proteinopathy.

Transgenic mice with doxycycline (Dox)-suppressible expression of human TDP-43 containing a defective nuclear localization signal ($hTDP-43^{\Delta NLS}$) under the control of the neurofilament heavy chain promoter (rNLS8 mice) are one of the most disease-relevant models of ALS, displaying progressive TDP-43 cytoplasmic accumulation coinciding with rapid ALS-like neurodegeneration and motor decline [18, 19]. In this study, we, therefore, screened for genes that may regulate and respond to cellular stress pathways in the cortex of rNLS8 mice prior to disease onset and throughout early disease stages. We thereby identified alterations in expression of several genes across multiple molecular pathways, including upregulation of genes involved in the ISR, DNA damage response, apoptosis, and neuroinflammation, and downregulation of genes involved in glycolysis and ion exchange, in the rNLS8 mouse cortex. Remarkably, several genes involved in the ISR, DNA damage response, and apoptosis were dramatically increased even prior to disease onset. Notably, anti- and pro-apoptotic genes were up-regulated prior to disease onset, with a switch towards solely pro-apoptotic signaling at later disease stages in rNLS8 mice. Our results also revealed a significant elevation of cleaved caspase-3 levels in late-disease rNLS8 mice, supporting ISR-mediated apoptosis as a critical contributor to neurodegeneration in disease. To investigate whether amelioration of ISR signaling could protect against disease, we, therefore, performed intracerebroventricular (ICV) injection of antisense oligonucleotides (ASOs) targeting Chop [20] to suppress Chop expression in rNLS8 mouse central nervous system. ASO treatment decreased Chop levels but did not affect overall TDP-43 pathology, neurodegeneration, gliosis, or motor deficits in rNLS8 mice. Taken together, we conclude that TDP-43 mislocalisation leads to early perturbation of multiple molecular pathways that crosstalk with ISR signals, with dysregulation of apoptosis signaling contributing to disease in rNLS8 mice.

MATERIALS AND METHODS
Animals
To generate samples for RT^2 qPCR arrays, rNLS8 transgenic mice and littermate controls on a mixed B6/C3H F1 background were produced as previously described [18]. Founder monogenic B6;C3-Tg(NEFH-tTA)8Vle/J (NEFH-tTA line 8, stock #025397) mice and monogenic B6;C3-Tg(tetO-TARDBP*)4Vle/J (tetO-hTDP-43$^{\Delta NLS}$ line 4, stock #014650) mice were obtained from the Jackson Laboratory (Bar Harbor, ME, USA) [19]. Intercross breeder and experimental mice were fed with chow containing 200 mg/kg doxycycline (Dox) (Specialty Feeds, Australia). Experiments were conducted with approval from the Animal Ethics Committee of Macquarie University (#2016-026). For all other experiments, rNLS8 mice were produced from the intercross of homozygous tetO-hTDP-43$^{\Delta NLS}$ line 4 mice with hemizygous NEFH-tTA line 8 mice both on a pure C56BL/6JAusb background following >10 generations of backcrossing and were fed with Dox-containing chow (200 mg/kg, Specialty Feeds, Australia) [21]. Experiments were conducted with approval from the Animal Ethics Committee of The University of Queensland (#QBI/131/18). During all experiments, mice were switched to normal chow to induce expression of $hTDP-43^{\Delta NLS}$. Male and female mice at approximately ten weeks of age were housed in temperature- and humidity-controlled conditions ($21 \pm 1\,°C$, $55 \pm 5\%$) with a 12 h light/dark cycle (lights on at 06:00 h). Mice were randomly allocated to groups for all experiments of time

point analyses and ASO administration groups, the size of which were calculated by G*Power (version 3.1). Both sexes were included and balanced between groups. Littermate non-transgenic and monogenic animals were used as controls. One mouse was excluded from all analyses due to non-neurological disease (malocclusion). Three mice in the ASO experiments were excluded from the qPCR and histological analyses since they reached the humane end-point prior to the predefined time point for tissue collection of 6 weeks off Dox. All experimental procedures were conducted under the guidelines of the National Health and Medical Research Council of Australia in accordance with the Australian Code of Practice for the Care and Use of Animals for Scientific Purposes.

Surgery procedures and ASO administration
Two Chop ASOs (known as Chop-ASO #3 and #5 respectively) were synthesised and purified as previously described [20, 22], with the ASO sequences shown in Table 1. For intracerebroventricular (ICV) injection, mice were anaesthetised by isoflurane (Abbott Laboratories) using an isoflurane machine (Kent Scientific Co. Torrington, CT, USAs) at the rate of 2–4% according to body weights of mice. Bilateral ICV injections were conducted stereotaxically using a 30 G needle connected to a Hamilton syringe by polyethylene tubing into lateral ventricles: anteroposterior = 0; lateral = ± 0.9; depth = 2.3 (coordinates are in millimetres relative to the Bregma) [23]. A total of 10 µL of ASO solution (50 mg/mL prepared in sterile saline solution) or saline solution as vehicle were injected into each of the left and right ventricles over 2 min (5 µL in each ventricle). After injections, mice were housed in home cages for two weeks before the removal of the Dox diet to induce neuronal $hTDP-43^{\Delta NLS}$ expression.

Mouse monitoring and behavioural tests
Mice were monitored and weighed three times per week after Dox feed was removed as previously described [18, 19]. Briefly, for observation of collapsing splay or clasping of hindlimbs, mice were suspended by the tail for >5 s. The failure to extend both hindlimbs was recorded as a positive response of collapsing splay and holding hindlimbs together was recorded as a presence of clasping splay. Mice were tested for rotarod performance of motor coordination and balance once per week, as previously described [19]. Briefly, mice were placed on a rotarod apparatus (Ugo Basile SRL, Gemonio, Italy) at a speed of 5 rpm with acceleration up to 40 rpm within 300 s. The time to fall was recorded. If mice were still running at the end of the testing session, their times were recorded as 300 s. Three training sessions were performed one week prior to time off Dox, and two test sessions were conducted weekly, with the final score being the highest time of the two test sessions. Experimenters were blinded to treatment group for hindlimb clasping and rotarod assessments.

RNA extraction
RNA was extracted from the homogenates of the rostral cortices (anteroposteriorly approximate 3.0 to −0.5 mm, Bregma) that contain the primary and secondary motor cortex or the lumbar spinal cord with Qiazol (Qiagen, #79306) using the Qiagen RNeasy Mini Kit (Qiagen, #74104) and Precellys tissue homogeniser (Bertin Instruments, Montigny-le-Bretonneux, France). On-column DNase I digestion was conducted using RNase-free DNase I (Qiagen, #79254). The concentration of extracted RNA was determined using a NanoRNA kit (Agilent, #5067-1511) and Bioanalyzer (Agilent 2100, Santa Clara, CS, USA). cDNA was synthesized from 1 µg total RNA using the SuperScript™ VILO™ Master Mix (Thermo Fisher, #11755050).

RT^2 PCR arrays and data analysis
RT^2 Profiler™ PCR Arrays (SABioscience Corporation, #PAMM-003Z) were used to detect differentially expressed cell stress and death genes of

Table 1. Sequences and details of the Chop ASOs.

ASO ID	Sequences	Effects	Chemical modifications	Reference
ASO#3*	CTAGATCCTTTCTAACTCCT	Knockdown of Chop gene	Central gap segment containing ten 2′- deoxyribonucleotides flanked at 5′ and 3′ with 2′MOE modified nucleotides; linkages with phosphodiester; all cytosines are 5′-methylcytosines.	[20, 22]
ASO#5	GATGCAATTTTTTATTTTTC	N/A		

*indicates that ASO#3 was used in the experiments in this study.

interest in the rostral cortices of control and rNLS8 mice at 2 and 4 weeks off Dox. The SYBR-Green based RT^2 PCR arrays contained 84 genes plus 5 housekeeping genes and assay controls. cDNA was mixed with SYBR-green as per manufacturer instructions and loaded onto a 384 well plate, with each gene was assessed in quadruplicate. RT^2 PCR arrays were performed on the Vii7 Real-Time PCR System (Applied Biosystems, Waltham, MA, *USA*). Fold-change analysis was performed using the ExpressionSuite Software (version 1.1), whereby each gene was determined by exponentiation of $2^{-\Delta\Delta Ct}$. A fold change of greater than 2 and $p < 0.05$ was deemed significant. The ß2 microglobulin (*B2m*) gene was excluded from the housekeeping genes in analysis as the expression of *B2m* gene was significantly increased in the cortex of rNLS8 mice off Dox compared to controls (Supplementary Fig. 1A), in line with previous findings [24].

For hierarchical clustering, fold change data of genes of interest was processed using the web-based Morpheus software (Broad Institute, Cambridge, MA, USA). Classification of differentially expressed genes was performed to indicate co-regulated and functionally related genes. Gene ontology (GO) and Kyoto Encyclopedia of Genes and Genomes (KEGG) pathway enrichment analyses was performed using Metascape (version 3.0) with default parameters (minimum overlap = 3, *p*-value cutoff = 0.01, and minimum enrichment = 1.5) [25]. Protein-protein interaction enrichment analysis was performed using the Molecular Complex Detection (MCODE) algorithm using Metascape to identify densely connected components from examined pathways with default parameters [26]. Venn diagrams were constructed using InteractiVenn [27]. Volcano plots were generated using Prism-GraphPad software (version 9).

Real-time quantitative PCR (qPCR) assay

Target gene real-time qPCR analyses were conducted using SYBR Green Master Mix (Bioline #BIO-98005) with the LightCycler® 480 System (Roche, Basel, Switzerland) to validate the RT^2 PCR array results. The relative changes in gene expression were calculated based on the housekeeping gene ß-actin (*Actb*) according to the $2^{-\Delta\Delta CT}$ method [28] and normalised to control or saline-treated control groups. The sequences of primers are available in Supplementary Table 1.

Protein extraction and immunoblotting (IB)

Mouse rostral cortices or lumbar spinal cords were collected for IB as described above and snap-frozen on dry ice. Tissues were then thawed on ice and homogenised in 5× v/w RIPA lysis buffer (50 mM Tris, 150 mM NaCl, 1% NP-40, 5 mM EDTA, 0.5% sodium deoxycholate, and 0.1% SDS, pH 8.0) containing 1 mM PMSF and protease and phosphatase inhibitor cocktails (Sigma, # 4906845001 and #11836170001) with three 1.4 mm Zirconium oxide beads (Bertin Instruments, #P000927-LYSK0-A) using Precellys tissue homogeniser (Bertin Instruments, #P000669-PR240-A). Samples were centrifuged at 4 °C, 100,000 *g* for 30 min, and the supernatant was taken as the RIPA-soluble fraction. The remaining pellet was washed with RIPA buffer as above, this supernatant was discarded, and the resulting pellet was dissolved in 5× v/w urea buffer (7 M urea, 2 M thiourea, 4% CHAPS, and 30 mM Tris, pH 8.5) using the Precellys homogeniser and centrifuged at 22 °C, 100,000 *g* for 30 min. This supernatant was taken as the RIPA-insoluble/urea-soluble fraction. Protein concentrations of the RIPA-soluble fractions were determined using the Pierce™ BCA Protein Assay Kit (ThermoFisher Scientific #23225).

Protein samples of RIPA-soluble or RIPA-insoluble/urea-soluble fractions were separated by electrophoresis (120 V for 90 min) on a polyacrylamide gel containing 12% acrylamide in the presence of reducing agent (2-mercaptoethanol, Sigma #63689). After SDS-PAGE, proteins were transferred to nitrocellulose membranes (LI-COR Biosciences #P/N926-31092) and incubated in blocking solution (5% (w/v) BSA, 0.05% (w/v) Tween-20 in TBS (TBST)) and then incubated overnight in primary antibody diluted in the blocking solution. Primary antibodies used for immunoblotting were rabbit anti-TDP-43 polyclonal antibody (PAb) for detecting both human and mouse TDP-43 (Proteintech #10782-2-AP, 1:2000), rat anti-phospho-S409/410 TDP-43 monoclonal antibody (MAb) (Biolegend # 829901, 1:1000), mouse anti-CHOP Mab (Invitrogen #MA1-250, 1:1000), a rabbit anti-caspase 3 for detection of cleaved forms of caspase-3 (Abcam #9664, 1:1000), mouse anti-GAPDH Mab (Proteintech #60004-1-Ig, 1:10,000), and rabbit anti-GAPDH PAb (Proteintech #10494-1-AP, 1:2000). The nitrocellulose membranes were washed with TBST and incubated with IRDye secondary antibodies (LI-COR Biosciences, 1:20,000) for 1 h. Protein bands were visualized using the Odyssey CLx Imaging System (LI-COR Biosciences, Lincoln, NE, USA) and quantified using Image Studio Lite software (LI-COR Biosciences, Lincoln, NE, USA). The relative changes of protein levels were calculated by quantifying the bands in RIPA soluble fractions relative to the band of the internal reference GAPDH protein, or by quantifying the bands in RIPA-insoluble/urea-soluble fractions relative to total protein and subsequently normalised to the control group or saline-treated control group.

Histology and immunofluorescence labeling (IF)

Mice were perfused using PBS followed by 4% paraformaldehyde (PFA). The rostral cortex and lumbar spinal cord tissues were rapidly dissected and post-fixed in 4% PFA for 1 h at room temperature and 4 °C overnight. Post-fixed tissues were rinsed in phosphate-buffered saline (PBS) pH 7.4, dehydrated with a series of increasing concentrations of ethanol, and then embedded in paraffin. Embedded tissues were sectioned at 10 µm thickness. For IF, paraffin-embedded sections were deparaffinised in xylene and rehydrated through a series of decreasing concentrations of ethanol. After rehydration, sections were subjected to antigen retrieval solution (10 mM sodium citrate, 0.05% Tween-20, pH 6.0) at 95 °C for 10 min and then were allowed to cool. Sections were then blocked in 1% BSA in PBS containing 0.25% (v/v) Triton X-100 (PBST) and incubated in primary antibodies overnight at 4 °C. Primary antibodies used for IF were rabbit anti-TDP-43 polyclonal antibody (PAb) for detecting pan-TDP-43 for both human and mouse TDP-43 (Proteintech #10782-2-AP, 1:1000), rat anti-glial fibrillary acidic protein (GFAP) Mab (ThermoFisher Scientific #13-0300, 1:500), and mouse anti-CHOP Mab (Invitrogen #MA1-250, 1:1000). Sections were then washed in PBST and incubated in fluorophore-conjugated secondary antibodies, including donkey anti-rat conjugated Alexa-488 (ThermoFisher Scientific #21208, 1:1000) and donkey anti-rabbit conjugated Alexa-647 (ThermoFisher Scientific #48272, 1:1000). Nuclei were stained using 4′,6-diamidino-2-phenylindole (DAPI, Sigma-Aldrich #D8417, 1:1000).

Fluorescence microscopy and Image analysis

Images for IF sections were acquired using an epifluorescence microscope Axio Imager (Zeiss) under x20 objective (0.8 NA / 0.55 mm WD), providing a pixel size of 0.323 µm using Zen imaging software (Zeiss). Images were background-corrected using ImageJ software with the rolling ball background subtraction algorithm and were then quantified for protein levels of TDP-43 using CellProfiler software (Broad Institute, version 4.2.1) as previously published [29].

Statistical analysis

For two-value data, statistical analyses were conducted using a two-tailed *t*-test. One-way ANOVA was used for analyses of datasets with three values with Bonferroni's post hoc test using Prism-GraphPad software (version 9). Statistical significance is indicated as $^*p < 0.05$, $^{**}p < 0.01$, and $^{***}p < 0.001$. All data are presented as mean±standard error of the mean (SEM).

RESULTS

Early activation of cell stress and death pathways in the cortex of rNLS8 mice

To determine how numerous cell stress and death pathways are regulated in the cortex of rNLS8 mice in early disease stages, we conducted RT^2 PCR arrays to assess the expression of critical genes at time of approximate disease onset (2 weeks off Dox, 2 WOD) and an early disease stage (4 weeks off Dox, 4 WOD) (Fig. 1A, Supplementary Fig. 2). We assessed 84 mouse genes in ten functional groups, with four housekeeping genes (*B2m* excluded; Supplementary Fig. 1A) and three negative controls (the full gene expression dataset is available in Supplementary Table 2). Firstly, we confirmed the expected increases of human *TARDBP* (*hTARDBP*) mRNA levels in the cortex of rNLS8 mice from 1 WOD (Supplementary Fig. 1B), prior to assessment of cell stress gene changes, as well as at 2 and 4 WOD (Fig. 1B) relative to control mice, using real-time qPCR. Notably, the level of *hTARDBP* mRNA was apparently higher in the cortex (Fig. 1B, Supplementary Fig. 1D) than in the spinal cord (Supplementary Figs. 1C, 1E) of rNLS8 mice, consistent with our previous observation of higher hTDP-43$^{\Delta NLS}$ protein levels and earlier accumulation of TDP-43 pathology in the cortex than in the spinal cord in this model [19]. In contrast, the mRNA levels of mouse *Tardbp* (*mTardbp*) were unchanged in rNLS8 mice compared to controls at 2 and 4 WOD (Fig. 1B), potentially due to the lack of sensitivity in this bulk tissue

Fig. 1 (A–G) Experimental design and gene expression analysis in rNLS8 mice.
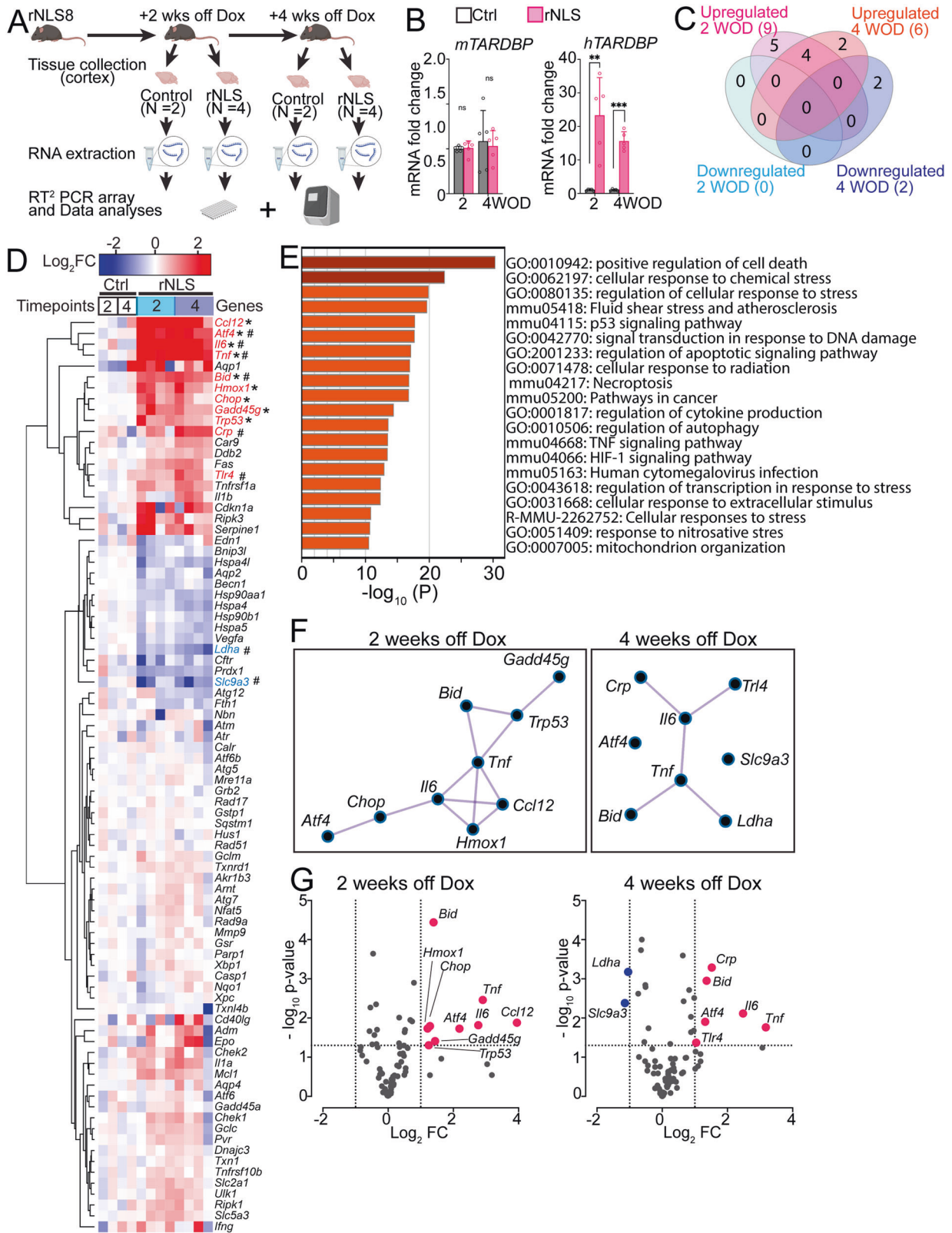
analysis to detect the expected auto-regulatory loss of *mTardbp* in neurons at these timepoints. However, as expected, *mTardbp* levels were decreased in the cortex of rNLS8 at 6 WOD (Supplementary Fig. 1D). These findings are in line with previous reports that overexpression of *hTDP-43$^{\Delta NLS}$* decreases endogenous *mTardbp*

mRNA and mTDP-43 protein levels via an auto-regulatory mechanism [19, 30, 31].

At 2 weeks off Dox, taken as disease onset, we identified a total of nine statistically significantly upregulated genes (fold change >2, $p < 0.05$) in the rNLS8 mice (Fig. 1C, the expression dataset of

Fig. 1 Cellular stress and death signaling pathways are activated in the cortex of rNLS8 mice at early disease stages. A Experimental schema. **B** Real-time qPCR analysis of mouse *Tardbp* and human *TARDBP* gene expression in the cortex of rNLS8 mice at 2 and 4 weeks off Dox (WOD) relative to controls. $n = 5$. Mean ± SEM. [**]$p < 0.01$ and [***]$p < 0.001$. **C** Total number of unique and shared statistically significantly upregulated or downregulated genes in rNLS8 mice at each time point, relative to the control mice. **D** Unsupervised hierarchical clustering heatmap for expression of all assayed genes in RT[2] PCR array from rNLS8 and control mice at each timepoint, with values given as normalised gene expression levels ($\log_2$ fold changes). Statistically significantly ($p < 0.05$) upregulated and downregulated genes are indicated in red and blue, respectively. * indicates statistical significance for 2 WOD and # for 4 WOD. **E** Gene ontology enrichment analyses for all the genes of interest in RT[2] PCR arrays. **F** MCODE network analyses for protein-protein interaction of identified differentially expressed genes in rNLS8 mice at 2 and 4 WOD, respectively. **G** Volcano plots indicate the magnitude (x axis, as $\log_2$ fold changes) and statistical significance (y axis, as $-\log_{10}$ *p*-values) of gene expression changes in rNLS8 mice relative to control mice at each timepoint. Upregulated genes (fold change >2) are shown in red and downregulated genes (fold change < -2) are shown in blue.

Table 2. Genes showing statistical significant difference with >2-fold change in cortex of rNLS8 mice at 2 weeks or 4 weeks off Dox compared to controls detected on RT[2] PCR array.

Symbol	Unigene	Refseq	Description	2 weeks off Dox		4 weeks off Dox	
				Fold change relative to control mice	*p*-value	Fold change relative to control mice	*p*-value
Atf4	Mm.641	NM_009716	Activating transcription factor 4	4.6	0.01870	2.5	0.01253
Bid	Mm.235081	NM_007544	BH3 interacting domain death agonist	2.6	0.00004	2.6	0.00112
Ccl12	Mm.867	NM_011331	Chemokine (C-C motif) ligand 12	15.5	0.01318	8.4	0.05732
Crp	Mm.28767	NM_007768	C-reactive protein, pentraxin-related	1.4	0.28464	2.9	0.00051
Chop	Mm.110220	NM_007837	DNA-damage inducible transcript 3	2.3	0.01857	1.7	0.10291
Gadd45g	Mm.281298	NM_011817	Growth arrest and DNA-damage-inducible 45 gamma	2.7	0.03883	1.8	0.00933
Hmox1	Mm.276389	NM_010442	Heme oxygenase (decycling) 1	2.4	0.01609	2.3	0.08352
Il6	Mm.1019	NM_001314054	Interleukin 6	6.8	0.01527	5.6	0.00768
Ldha	Mm.29324	NM_010699	Lactate dehydrogenase A	0.7	0.00539	0.5	0.00066
Slc9a3	Mm.261564	NM_001081060	Solute carrier family 9 (sodium/hydrogen exchanger), member 3	0.6	0.05494	0.5	0.00415
Tlr4	Mm.38049	NM_021297	Toll-like receptor 4	1.4	0.02000	2.1	0.04270
Tnf	Mm.1293	NM_013693	Tumor necrosis factor	7.5	0.00347	9.0	0.01730
Trp53	Mm.222	NM_011640	Transformation related protein 53	2.4	0.04958	1.6	0.00374

identified genes is available in Table 2). At 4 weeks off Dox, taken as an early disease stage after accumulation of TDP-43 pathology, we detected six upregulated genes and two downregulated genes (fold change < -2, $p < 0.05$) in the rNLS8 mice relative to controls (Fig. 1C). Among these dysregulated genes, we identified four genes that were upregulated at both 2-week and 4-week timepoints in the cortex of rNLS8 mice in the RT[2] array, namely activating transcription factor 4 (*Atf4*), pro-apoptotic BH3 Interacting Domain Death Agonist (*Bid*), interleukin 6 (*Il6*), and tumor necrosis factor-alpha (*Tnf*). Consistent alteration in these pathways indicates involvement of these genes in disease over an extended period, suggesting that these pathways may be important for disease progression.

The hierarchical heatmap showing the magnitude of fold change in expression between rNLS8 mice and controls in the RT[2] array demonstrated a clear bi-clustering pattern of upregulated genes (in red) and downregulated genes (in blue) over the disease course (Fig. 1D). The GO enrichment analyses of all pre-selected genes revealed that the top three biological processes relate to ISR signaling: positive regulation of cell death (GO:0010942), cellular response to chemical stress (GO:0062197), and regulation of cellular response to stress (GO:0080135) (Fig. 1E). Furthermore, the

molecule complex detection (MCODE) network for protein-protein interaction revealed significant interactions of identified genes among biological processes, notably the positive regulation of cell death via the ATF4-CHOP axis of the ISR in the disease-onset rNLS8 mice at 2 weeks off Dox (Fig. 1F).

To further interrogate the gene changes in rNLS8 mice, we grouped analysed genes based on biological pathway at both 2-week and 4-week timepoints. At 2 weeks off Dox, upregulated genes act within several pathways: the ISR, being *Atf4* (~3.7 fold increased in rNLS8 mice) and C/EBP homologous protein (*Chop*, ~2.3 fold); apoptosis signaling, being *Bid* (~2.6 fold); oxidative stress response, being Heme Oxygenase 1 (*Homx1*, ~2.4 fold); DNA damage response, being DNA Damage Inducible Gamma (*Gadd45g*, ~2.7 fold) and transformation related protein 53 (*Trp53*, ~2.3 fold); neuroinflammation, being chemokine (CC motif) ligand 12 (*Ccl12*, ~15.5 fold) and *Il6* (~6.7 fold), and; TNF family signaling, being *Tnf* (~7.4 fold) (Supplementary Fig. 2). The data suggest that TDP-43 cytoplasmic mislocalisation in neurons of rNLS8 mice results in disruption of cellular homeostasis including ISR activation, DNA damage, oxidative stress, and neuroinflammation as early as disease onset.

At 4 weeks off Dox, upregulated genes largely belong to the same biological pathways as at 2 weeks: the ISR, being *Atf4* (~ 2.5 fold increased in rNLS8 mice); apoptosis signaling, being *Bid* (~2.5 fold); neuroinflammation, being the C-reactive protein gene (*Crp*, ~2.8 fold), Il6 (~ 5.5 fold), and the Toll-like receptor 4 gene (*Tlr4*, ~2.1 fold), and; TNF family ligand, being *Tnf* (~ 9.0 fold) (Supplementary Fig. 2). Furthermore, we also identified two downregulated genes in the cortex of rNLS8 mice at 4 weeks off Dox that were not altered at 2 weeks, involved in: cellular metabolism (glycolysis), being lactate dehydrogenase A (*Ldha*, ~ 0.5 fold), and; ion metabolism, being the solute carrier family 9 member A3 (*Slc9a3*, ~0.5 fold) (Supplementary Fig. 2). These results suggest there is a prolonged elevation of cell stress response during disease and later dysregulation in cellular metabolism in the rNLS8 mice.

To validate our findings in RT^2 array analyses and determine whether changes occur even before disease onset, we conducted real-time qPCR for all 13 genes detected as significantly altered in at least one of the timepoints in the rNLS8 mice, in separate experiments using an independent set of mouse cortex samples. In addition to disease onset (2 weeks) and early disease (4 weeks) timepoints, we additionally analysed samples from mice prior to disease onset (1 week off Dox), a timepoint at which rNLS8 mice display increased cytoplasmic human TDP-43 protein levels but no overt motor phenotypes [19]. Intriguingly, five of the 11 upregulated genes originally identified as altered in array data were already upregulated at 1 week timepoint (Fig. 2A), including genes involved in: the ISR, being *Atf4* (~1.5 fold) and *Chop* (~2.1 fold); apoptosis signaling, being *Bid* (~2.2 fold), and; DNA damage response, being *Gadd45g* (~1.4 fold) and *Trp53* (~1.7 fold). Expression of these five genes were also consistently elevated at 2 weeks and 4 weeks off Dox relative to the control mice, consistent with the array findings. Moreover, qPCR results showed consistent up-regulation of selected genes in rNLS8 mice on both the original mixed B6/C3H background (Supplementary Fig. 3A), as employed in the RT^2 array, and on pure C56BL/6JAusb background (Fig. 2A), as employed in the following experiments. Consistent upregulation of these genes suggests the early and prolonged activation of cellular stress pathways and pro-apoptosis signaling in the cortex of rNLS8 mice upon the induction of *hTDP-43^{ΔNLS}* expression, even before disease onset.

Given the prominence of changes in the ISR pathway early in the rNLS8 mice, we also examined changes in additional ISR genes not included in the array data, including levels of protein phosphatase 1 regulatory subunit 15 A mRNA (*Ppp1r15a*) gene encoding GADD34 that is the direct target of ISR-ATF4-CHOP axis [11], and mRNA splicing of X-box binding protein 1 (*Xbp1*) that is a potent transcription factor under regulation of the inositol-requiring enzyme 1 (IRE1) branch of unfolded protein response (UPR) [12]. Notably, we identified upregulation of the *Ppp1r15a* gene (~ 1.4 fold, Fig. 2B) at 1-week timepoint, but not 2- or 4-week timepoint, suggesting impairment of GADD34-mediated negative feedback regulation of the ISR. As expected, the total and unspliced *Xbp1* mRNAs showed no significant differences between groups (Fig. 2B), in line with the array data for total *Xbp1* mRNAs (Supplementary Fig. 2A). However, there was marked elevation of spliced (active) *Xbp1* mRNA (~ 2.2 fold) in rNLS8 mice at the 1-week and 2-week timepoints. Overall, these findings indicate the early activation of the ISR and broader UPR signaling from the beginning of induction of *hTDP-43^{ΔNLS}* expression in rNLS8 mice, with later loss of this potentially protective response during disease progression.

In line with the RT^2 array data, we confirmed the mRNA levels for five further upregulated genes that were significantly increased in the cortex of rNLS8 mice at 2- and 4-week timepoints compared to control mice (Fig. 2C), including those involved in: neuroinflammation, being *Ccl12*, *Il6*, *Tnf*, and *Trl4*, and oxidative stress response, being *Homx1*. Notably, the expression of these five genes was not significantly different between rNLS8 and

control mice at the 1-week timepoint, suggesting that activation of neuroinflammation and the oxidative stress response may be later events than ISR and apoptotic signaling in the cortex of rNLS8 mice.
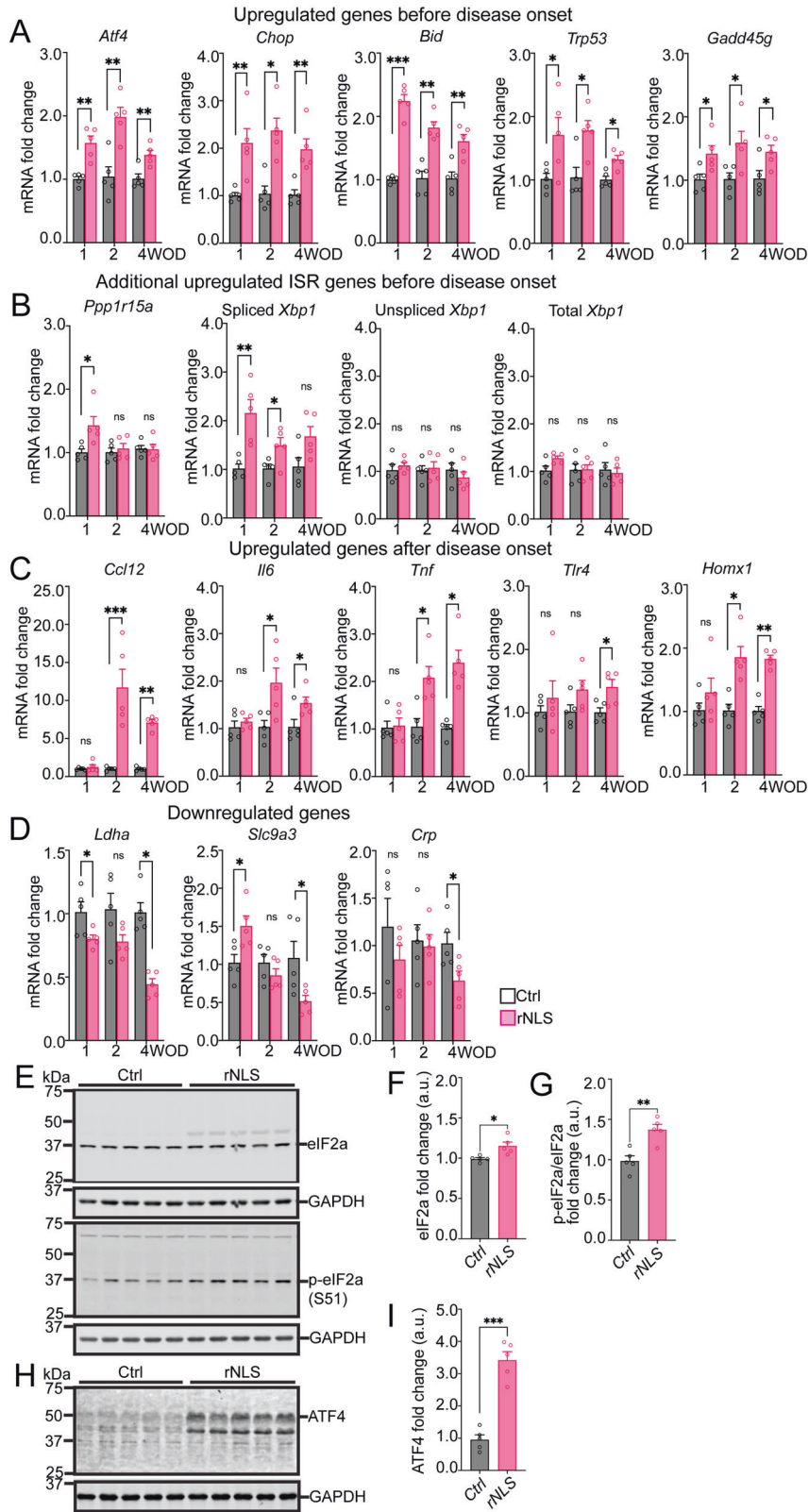
Concerning the two genes identified as downregulated in the RT^2 array data, we verified the downregulation of *Ldha* and *Slc9a3* genes in the cortex of rNLS8 mice compared to the control mice at the 4-week timepoint (Fig. 2D). Unexpectedly, although both genes were not different between groups at the 2-week timepoint, we also detected a decrease of *Ldha* mRNA in the cortex of rNLS8 mice relative to control mice at the 1-week timepoint, suggesting early deficiency in metabolism may occur in rNLS8 mice. In contrast, we observed a significant *increase* of *Slc9a3* mRNA at the 1-week timepoint compared to control mice, suggesting that effects of disruption of sodium absorption may change over time in rNLS8 mice. Surprisingly, we detected a decrease of neuroinflammatory *Crp* mRNA in the cortex of rNLS8 mice at the 4-week timepoint in qPCR results, in contrast to the increase of *Crp* in the RT^2 array, suggesting that changes in this gene may not be a consistent feature of disease in the rNLS8 mice (Fig. 2D). Together, these findings reveal involvement of several important pathways, most notably activation of the ISR, beginning even prior to disease onset and persisting throughout early disease stages in rNLS8 mice.

To investigate whether the detected changes in the rNLS8 mouse cortex were also reflected in the spinal cord, we assessed the levels of a select set of seven of the genes that were increased in rNLS cortex, in 2-week spinal cord tissues using qPCR. Notably, at this timepoint, the levels of *Chop*, *Atf4*, *Bid*, *Trp53* and *Gadd45g*, which were increased from 1-week in the cortex, and of *Il6*, which was increased from 2 weeks in the cortex, were unaltered in rNLS8 mouse spinal cord compared to controls at 2 weeks (Supplementary Fig. 3B). However, *Ccl12* levels were dramatically increased in 2-week rNLS8 mouse spinal cord (Supplementary Fig. 3B). These findings suggest that the very early alterations in ISR and apoptotic signaling seen in the cortex are not necessarily reflected at the early disease stages in the spinal cord of rNLS8 mice, although neuroinflammatory signals including increased levels of *Ccl12* are apparent.

To further biochemically validate activation of the ISR, we conducted immunoblotting (IB) to assess the phosphorylation of the eukaryotic initiation factor 2α (p-eIF2α) at serine 51 (S51), the core effector of the ISR, and the selective downstream target ATF4 protein [11] in rNLS8 mice at early disease stage (4 week timepoint). The IB results revealed slight but significant increases of eIF2α protein (~1.1 fold, Fig. 2E, F) and significant increases of p-eIF2α (S51) (~1.4 fold, Fig. 2E, G) in the cortex of rNLS8 mice compared to control mice at the 4 week timepoint. Notably, we also detected a dramatic increase of ATF4 protein (~3.8 fold, Fig. 2H, I) in rNLS8 mice relative to control mice. These data further confirm activation of the ISR caused by accumulation of TDP-43 pathology in rNLS8 mice at early disease stages.

Antisense oligonucleotide-mediated knockdown of *Chop* does not ameliorate motor deficits in rNLS8 mice

Apoptosis has been proposed as the final pathway leading to neurodegeneration in ALS and FTD [10]. Our array and qPCR results revealed consistent upregulation of *Atf4*, *Chop*, and also *Bid* (an apoptotic gene downstream of ISR-ATF4-CHOP signaling) in the cortex of rNLS8 mice as early as 1 week off Dox, suggesting that ISR-mediated apoptosis may be a pathogenic mechanism associated with TDP-43 pathology. CHOP protein not only converges upstream multiple stress signals such as ISR [11, 12], DNA damage [32] and inflammation [33], which we found to be dysregulated in rNLS8 mice (Fig. 2), but CHOP also acts as a critical transcription factor to directly regulate the expression of downstream apoptosis genes and to coordinate the initiation of the apoptosis cascade [13]. Importantly, previous evidence indicates

A Upregulated genes before disease onset

B Additional upregulated ISR genes before disease onset

C Upregulated genes after disease onset

D Downregulated genes

that knockdown of *Chop* gene using shRNA can inhibit neuronal apoptosis [34]. Therefore, we selected *Chop* as the target gene to manipulate inhibition of apoptotic signaling in rNLS8 mice, aiming to protect neurons against cell death and thereby prevent motor deficits. Previously, several RNase H-gapmer ASOs were reported

to specifically target the *Chop* gene, successfully decreasing levels of CHOP protein in cells and mice [20]. We thus examined the efficacy of these previously reported *Chop* ASOs [20], and selected the most effective *Chop* ASO (previously reported as ASO#3), which suppressed *Chop* gene expression in the cortex of rNLS8

Fig. 2   rNLS8 mice display dysregulation of genes in multiple cellular stress pathways and activation of the ISR in the cortex even prior to disease onset. A Real-time qPCR verified upregulated RT^2 array-identified genes (*Atf4, Chop, Bid, Trp53* and *Gadd45g*) in the cortex of rNLS8 mice at 2 and 4 weeks off Dox (WOD), and revealed similar upregulation at 1 WOD. **B** Additional ISR-related genes (*Ppp1r15a* and spliced *Xbp1*) were also upregulated at 1 WOD. **C** The RT^2 array-identified upregulated genes *Ccl12, Il6, Tnf, Tlr4* and *Homx1* were verified as increased at 2 and 4 WOD but were unaltered at 1 WOD. **D** Differential alterations were also identified in the RT^2 array-identified downregulated genes (*Lhda, Slc9a3* and *Crp*) at 1 and 4 WOD. Values were normalized to *Actb* as the housekeeping gene. **E** Immunoblotting for the proteins of eIF2α and p-eIF2α (S51) in the cortex of rNLS8 mice at 4 WOD. Approximate molecular weights (kDa) are indicated. Quantification of immunoblots showed increased eIF2α (**F**) and p-eIF2α (**G**) in the cortex of rNLS8 mice relative to control mice, respectively. **H** Immunoblotting for ATF4 protein in the cortex of rNLS8 mice at 4 WOD. **I** Quantification of immunoblots showed increased ATF4 protein in the cortex of rNLS8 mice relative to control mice. $n = 5$. Mean ± SEM. $^*p < 0.05$, $^{**}p < 0.01$, $^{***}p < 0.001$.

mice relative to control levels (Supplementary Fig. 4), for subsequent experiments in rNLS8 mice.

To investigate the effect of knockdown of *Chop* in rNLS8 mice, we conducted bilateral ICV injection of *Chop* ASO or its vehicle (saline) to adult littermate control or rNLS8 mice (10 weeks old), two weeks prior to Dox removal to ensure that decreased *Chop* mRNA occurred from the beginning of induction of *hTDP-43^{ΔNLS}* expression (Fig. 3A). We examined neurological and behavioural phenotypes, TDP-43 pathology, and motor neurodegeneration in treated mice. Firstly, qPCR showed significantly higher (by ~1.5 fold) *Chop* mRNA levels in the cortex of saline-treated rNLS8 mice (referred as the rNLS-Sal group) at mid-disease stage of 6 weeks off Dox (eight weeks after ICV injection of ASOs), compared to the saline-treated control mice (the Ctrl-Sal group) (Fig. 3B). The data indicate that the early increases in *Chop* mRNA previously detected from 1 week off Dox continued until at least this later disease state at 6 weeks off Dox. The qPCR data also confirmed that *Chop* ASO successfully decreased the *Chop* mRNA in the cortex in rNLS8 mice (the rNLS-ASO group), to approximately the level of control saline-injected mice (Fig. 3B). Although there were no significant differences in the mRNA levels of *Chop* in the spinal cord between Ctrl-Sal and rNLS-Sal mice, *Chop* was decreased by ~40% in the spinal cord of the rNLS-ASO group compared to the Ctrl-Sal or rNLS-Sal groups (Fig. 3B), indicating that direct ICV injection of *Chop* ASO can effectively decrease both cortex and spinal cord *Chop* gene expression.

Furthermore, we conducted immunoblotting to analyse CHOP protein levels in the cortex and spinal cord of rNLS8 mice after ASO treatment (Fig. 3C). Despite difficulties in detecting this protein via immunoblotting, we identified significant elevation of CHOP protein in the cortex of the rNLS8 mice (rNLS-Sal) of approximately 2.1-fold compared to the control (Ctrl-Sal), with a trend for a decrease in CHOP protein in rNLS-ASO mice (approximately 1.6-fold compared to rNLS-Sal mice), although this decrease did not reach statistical significance (Fig. 3D). CHOP protein levels were difficult to detect in the spinal cord and there were no apparent differences in the levels of CHOP protein in the spinal cord of treatment groups despite the decrease detected via qPCR, although there was substantial variation in detected protein levels between mice (Fig. 3D). Immunofluorescence of the motor cortex in mice at 6 weeks off Dox indicated that increased CHOP protein was primarily localized to neurons expressing hTDP-43^{ΔNLS}, with some additional surrounding non-neuronal cells also showing increased CHOP levels in rNLS8 mice (Supplementary Fig. 5). Overall, consistent with previous evidence for a successful decrease of CHOP protein upon treatment with the ASO used here [20], our results confirmed successful knockdown of *Chop* in the nervous systems of rNLS8 mice.

We further examined the effects of knockdown of *Chop* gene on neurological phenotypes of rNLS8 mice until late disease stages. rNLS8 mice developed characteristic features of progressive neurological decline compared to control mice, including hind-limb clasping onset (Fig. 3E) and progressive motor dysfunction (Fig. 3F), and body weight loss (Fig. 3G), similar to results previously reported in mixed B6/C3H background [19] and recently in pure C56BL/6JAusb background [21]. Notably, *Chop*

ASO treatment had no significant effects on any of the examined neurological phenotypes (Fig. 3E–G). Further, there was no difference in the number of rNLS-ASO mice remaining on-study at 6 weeks off Dox compared to the rNLS-Sal mice (Fig. 3H), although later disease stages were not assessed. Lastly, *Chop* ASO did not significantly affect the expression of genes identified by RT^2 array in the cortex or spinal cord of treated mice comparing to the rNLS-Sal mice (Supplementary Fig. 6). Overall, these results demonstrate that knockdown of *Chop* gene did not affect the onset or early progression of motor phenotypes in rNLS8 mice.

Knockdown of *Chop* does not alter overall TDP-43 pathology in rNLS8 mice

As TDP-43 pathology, such as cytoplasmic aggregation, modification and phosphorylation, is the critical pathological feature of ALS and FTD [1, 5], we next examined the outcomes of knockdown of *Chop* on TDP-43 pathology in treated rNLS8 mice by assessing the levels of overall soluble and insoluble TDP-43 protein, TDP-43 fragments, and pTDP-43. We detected significant increases of total TDP-43 protein (human and mouse TDP-43) in the RIPA-soluble fractions of cortex (Figs. 3I, J) and spinal cord (Figs. 3M, N) of rNLS-Sal mice compared to the Ctrl-Sal group, as expected. However, *Chop* knockdown caused no significant changes to the levels of RIPA-soluble total TDP-43 protein in cortex (Figs. 3I, J) or spinal cord (Figs. 3M, N) of rNLS8 mice compared to the rNLS-Sal group. The levels of total TDP-43 protein were also dramatically increased in the RIPA-insoluble fraction of both cortex (Figs. 3I, K) and spinal cord (Figs. 3M, O) of the rNLS-Sal mice relative to Ctrl-Sal mice, as seen previously [19]. Notably, we detected accumulation of RIPA-soluble and -insoluble TDP-43 C-terminal fragments (CTFs) in the rNLS8 mice with the antibodies and conditions used in this study (Figs. 3I, M), in contrast to the original report of this model [19]. *Chop* knockdown had no effect on levels of total, CTF or high-molecular weight TDP-43 in the RIPA-insoluble fraction in the cortex of rNLS8 mice (Figs. 3I, K), and there was similarly no effect on total or the high-molecular weight TDP-43 species in the RIPA-insoluble fraction in the spinal cord of rNLS8 mice (Figs. 3M, O). However, interestingly, the spinal cord samples from rNLS-ASO mice showed a modest but statistically significant decrease in the low-molecular-weight TDP-43 CTFs (20–37 kDa) compared to rNLS-Sal mice (Fig. 3O). We further examined levels of pTDP-43 at serines 409/410 in the RIPA-insoluble protein fractions, demonstrating significant increases of pTDP-43 in both cortex (Fig. 3L) and spinal cord (Fig. 3P) of the rNLS-Sal mice compared the Ctrl-Sal mice, as expected. Nevertheless, knockdown of *Chop* did not change the levels of pTDP-43 in either cortex or spinal cord of rNLS8 mice.

To further analyse the effect of *Chop* knockdown on TDP-43 accumulation in the cytoplasm of neurons in rNLS8 mice, we conducted IF for TDP-43 and analysed neurons in the cortex (Fig. 3Q) and spinal cord (Fig. 3R), with TDP-43 primarily localised in the nuclei of neurons of the Ctrl-Sal mice. In contrast, TDP-43 was localised to cytoplasmic regions in the neurons in the layer V of the cortex (Fig. 3Q), and neurons in the ventral horn of the lumbar spinal cord in rNLS8 mice (Fig. 3T), as expected [19].
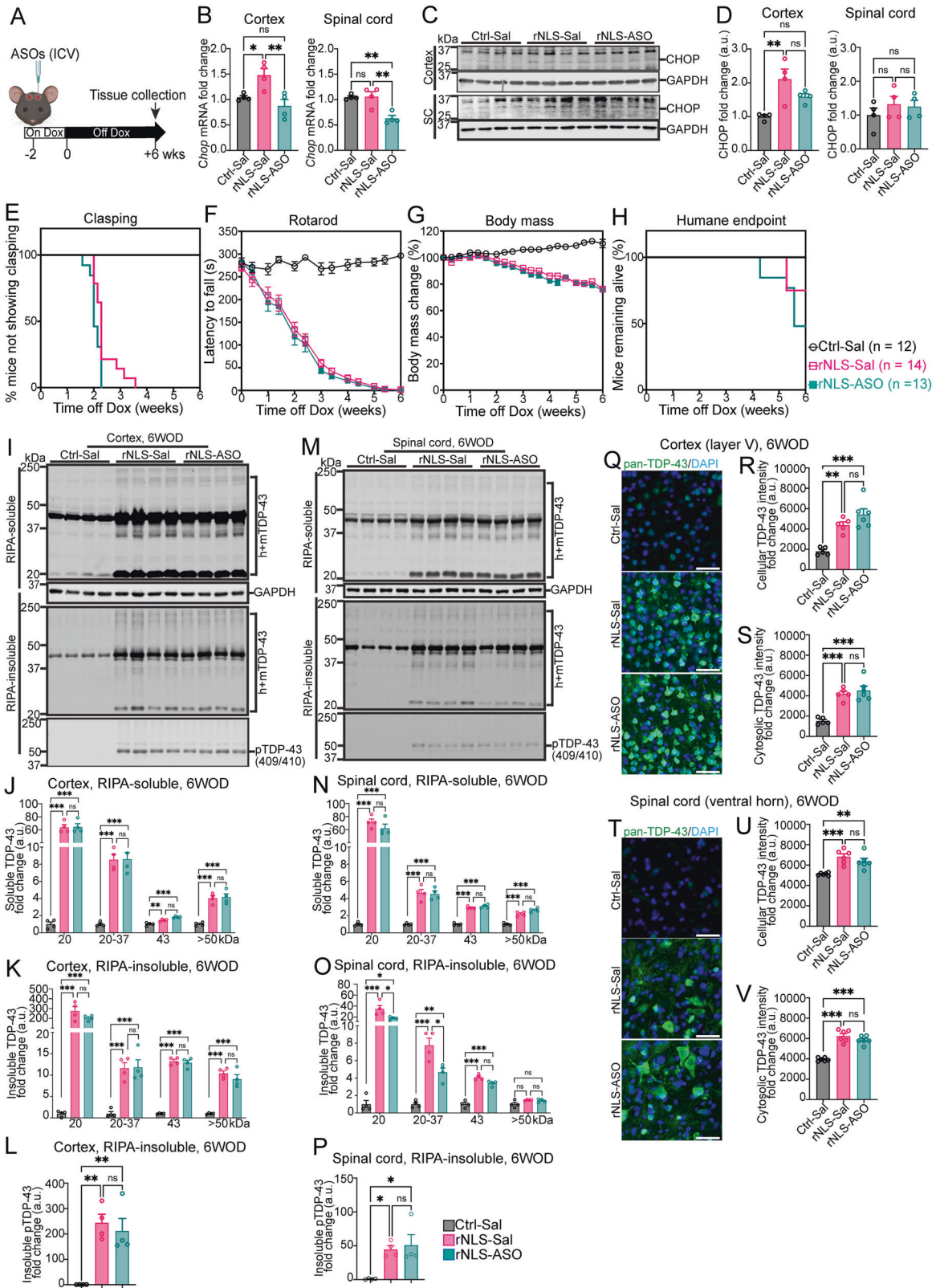
Nevertheless, *Chop* ASO treatment did not result in any changes in overall levels or cytoplasmic TDP-43 distribution in neurons of cortex or spinal cord in rNLS8 mice. Quantification of IF confirmed the elevation of TDP-43 in the rNLS-Sal and rNLS-ASO mice shown as fluorescence intensity measured per cell or within the cytosolic regions in cortical (Figs. 3R, S) and spinal cord neurons (Figs. 3U, V). Nevertheless, suppression of *Chop* by ASO led to no significant differences in total or cytosolic fluorescence intensity of TDP-43 between rNLS-Sal and rNLS-ASO groups. Overall, these data demonstrate that knockdown of *Chop* did not consistently affect

Fig. 3 **CHOP protein levels are increased in rNLS8 mice at 6 weeks off Dox, but ASO-mediated knockdown of *Chop* prior to induction of *hTDP-43$^{\Delta NLS}$* expression does not alter disease phenotypes or TDP-43 levels or solubility. A** Experimental schema. **B** Real-time qPCR assessment demonstrated *Chop* ASO decreased *Chop* mRNA levels in the cortex and spinal cord of treated rNLS8 mice at 6 weeks off Dox (WOD) ($n = 4$). Data are normalised to *Actb* as the housekeeping gene. **C** Immunoblotting for levels of CHOP protein in the cortex and spinal cord of treated rNLS8 mice at 6 WOD ($n = 4$). Approximate molecular weights (kDa) are indicated. **D** Quantification of immunoblots showed increased CHOP protein in the cortex and a trend of decrease of CHOP protein with ASO treatment in rNLS8 mice at 6 WOD. However, there were no significant differences between groups in CHOP protein levels in the lumbar spinal cord. **E–G**. Compared to saline-treated rNLS8 mice (rNLS-Sal), *Chop* ASO treatment led to no apparent beneficial effects on pathological phenotypes and motor deficits in clasping or rotarod test and did not alter the decline of body mass or affect the number of mice that had not reached humane endpoint by 6 WOD: with no mice reaching humane endpoint in Ctrl-Sal group ($n = 12$), three mice reaching humane endpoint in rNLS-Sal group ($n = 14$), and six mice reaching humane endpoint in rNLS-ASO group ($n = 13$) (**H**). IB assessed TDP-43 in the RIPA-soluble and RIPA-insoluble fractions and p-TDP-43 in the RIPA-insoluble fractions for the cortex (**I–L**) and spinal cord (**M–P**) of mice at 6 WOD ($n = 4$). Approximate molecular weights (kDa) are indicated on the left and target protein on the right. GAPDH was used as the loading control for RIPA-soluble IB and total protein for RIPA-insoluble IB. Quantification of IB for different molecular weight species of TDP-43 or p-TDP-43 in the RIPA-soluble and -insoluble fractions in the cortex (**J–L**) and the spinal cord (**N–P**) ($n = 4$). Representative IF images for pan-TDP-43 staining (human+mouse) (green) with the nuclear marker DAPI (blue) in the cortex (**Q**) and spinal cord (**T**) of treated mice at 6 WOD. Scale bars represent 50 μm. Quantification of IF for pan-TDP-43 protein in identified cell or cytoplasmic region in the cortex (**R, S**) and spinal cord (**U, V**) of treatment groups. Ctrl-Sal ($n = 5$), rNLS-Sal ($n = 6$) and rNLS-ASO ($n = 6$). Mean ± SEM. $^{*}p < 0.05$, $^{**}p < 0.01$ and $^{***}p < 0.001$.

the overall accumulation or mislocalisation of TDP-43 in rNLS8 mice.

rNLS8 mice display changes in apoptosis signaling over time and increased cleaved caspase-3 levels that are not affected by knockdown of *Chop*

It remains unclear how TDP-43 pathology affects the regulation of the downstream apoptotic mediators of CHOP activation. Thus, we first examined the expression of these apoptotic genes in rNLS8 mice at early disease stages. The qPCR results revealed significant elevation of anti-apoptotic *Bcl2* gene (~1.3 fold, Fig. 4A), Bcl2 homology 3 (BH3)-only pro-apoptotic initiator *Bim* gene (~1.5 fold, Fig. 4B) and *Noxa* gene (~2.2 fold, Fig. 4C) in the cortex of rNLS8 mice before disease phenotypes at 1 week off Dox, compared to control mice. There were no significant changes in *Bcl2* or *Bim* mRNAs at 2 or 4 weeks off Dox in rNLS8 mice, although upregulation of *Noxa* mRNA was detected at 2 weeks but not 4 weeks off Dox in rNLS8 mice (Fig. 4C). Notably, *Puma* mRNA level was not altered at 1 week off Dox but was significantly increased in the rNLS8 mice at 2- and 4-week timepoints, after disease onset (Fig. 4D). Dysregulation of these apoptosis genes suggests involvement of apoptosis signaling in neurodegeneration caused by TDP-43 pathology in rNLS8 mice, and suggests a differential switch from early competition between anti- and pro-apoptotic signals to later elevation of pro-apoptotic signaling at later disease phases.

Further, we assessed the expression of these apoptotic genes in rNLS8 mice at the mid-stage of disease (6 weeks off Dox) and with knockdown of *Chop*. Interestingly, we detected significantly decreased mRNA levels of the anti-apoptotic *Bcl2* gene as well as pro-apoptotic *Bim* and *Noxa* genes, and no difference in *Puma* mRNAs, in the cortex of the rNLS-Sal mice compared to the Ctrl-Sal mice at 6 weeks off Dox (Fig. 4E). This is in contrast to the upregulation of these genes identified at earlier disease stages of rNLS8 mice, and may be due to extensive neurodegeneration that occurs at this stage of disease [19]. Notably, *Bid* expression, which was upregulated in rNLS8 mice at early disease stages (1, 2 and 4 weeks off Dox, Fig. 2A), was not significantly different between control mice (Ctrl-Sal) and rNLS8 mice at this later disease stage (6 weeks off Dox). rNLS8 mice also displayed no alteration of examined genes in the spinal cord relative to the control mice (Ctrl-Sal) at 6 weeks off Dox (Fig. 4F). Further, *Chop* knockdown had no effect on the mRNA levels of anti- or pro-apoptosis genes in either cortex or spinal cord of treated mice at 6 weeks off Dox (Figs. 4E, F).

Given that caspases play essential roles in orchestrating apoptosis and caspase-3 is a primary downstream executioner among these proteases, we also examined the activation of

caspase-3 in the cortex of rNLS8 mice by quantifying the levels of a specific 17 kDa caspase-3 cleavage product (Fig. 4G), which is required for caspase-3 activity in apoptosis [35]. We detected a significant elevation of cleaved caspase-3 (~17 kDa band) in the cortex of the rNLS8 mice (rNLS-Sal) compared to the control mice (Ctrl-Sal) at the 6-week timepoint (Fig. 4H), suggesting that activation of apoptosis may drive neurodegeneration in the later stages of disease in rNLS8 mice. Similarly, there was a trend of increased cleaved caspase-3 levels in the spinal cord of rNLS8 mice (rNLS-Sal) relative to the control mice (Ctrl-Sal), although it did not reach statistical significance (Fig. 4H). Elevation of cleaved caspase-3 is consistent with the previous report that demonstrated dramatic motor neuron loss in the cortex of rNLS8 mice at 6 weeks off Dox [19]. Nevertheless, knockdown of *Chop* had no effect on the level of cleaved caspase-3 in either cortex or spinal cord of treated mice (rNLS-ASO) relative to the rNLS-Sal group (Fig. 4H). Overall, these data demonstrate that knockdown of *Chop* did not ameliorate the disease-associated activation of apoptosis signaling in rNLS8 mice, suggesting that alternative modulators or pathways may account for the upregulation of these apoptosis genes caused by TDP-43 pathology.

rNLS8 mice display dramatic astrogliosis and dysregulation of astrocytic genes, which are not ameliorated by knockdown of *Chop*

In addition to the cell-autonomous effect of ISR in neurons, dysfunctional astrocytes can also contribute to the pathogenesis of human neurodegenerative diseases [36]. Given that astrogliosis is an established feature of both ALS [37] and the rNLS8 mouse model [19], we assessed the activation of astrocytes that contribute to glutamate-induced motor neuron death in ALS [38] and which would be expected to be ameliorated by a beneficial treatment strategy. Firstly, we assessed astrocytes using the pan-reactive astrocytic marker GFAP by IF (Figs. 5A, D). The results indicated a dramatic increase in the number of GFAP-positive astrocytes with ramified cell processes in the cortex and spinal cord of rNLS8 mice (rNLS-Sal) compared to the Ctrl-Sal mice (Fig. 5B). Knockdown of *Chop* slightly but significantly increased the number of reactive astrocytes in treated mice (rNLS-ASO) relative to that of rNLS-Sal mice (Fig. 5B), with a slight elevation of GFAP intensity in the cortex of rNLS-ASO mice compared to the control mice (Ctrl-Sal) (Fig. 5C). However, we found no difference in either astrocyte number (Fig. 5E) or GFAP intensity (Fig. 5F) in the spinal cord among treatment groups despite a trend for increase in rNLS8 mice.

The ISR has been shown to impair the neurotrophic function and to modulate inflammatory states of astrocytes, by dysregulation of astrocytic gene expression [39]. Therefore, to determine whether knockdown of *Chop* affected the expression of genes
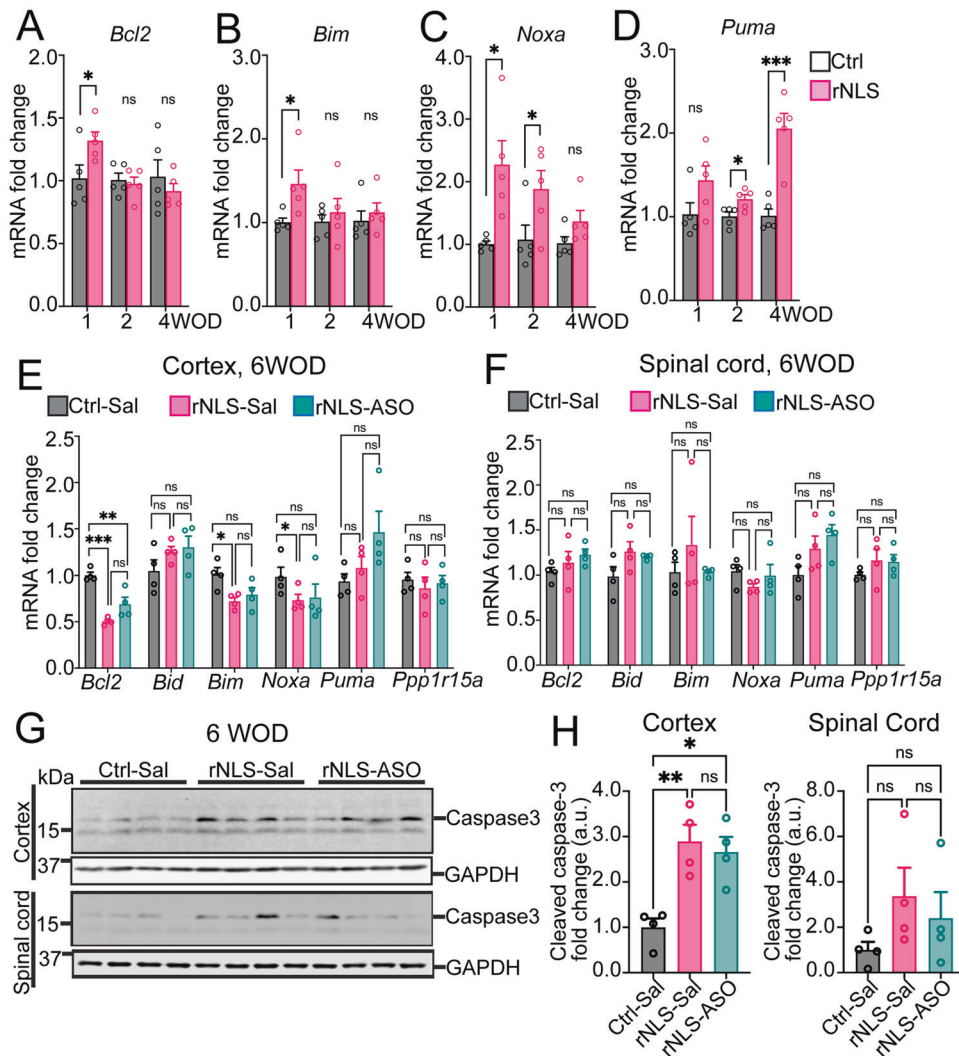
Fig. 4 rNLS8 mice display early activation of apoptosis, and increased cleaved caspase-3 levels in the cortex that is not altered by knockdown of *Chop*. Real-time qPCR results revealed dysregulation of *Chop* target apoptosis genes in the cortex of rNLS8 mice at 1, 2 and 4 weeks off Dox (WOD) (*n* = 5): **A** *Bcl2*; **B** *Bim*; **C** *Noxa*; **D** *Puma*. Real-time qPCR results revealed expression changes of CHOP downstream genes in (**E**) and spinal cord (**F**) of mice at 6 WOD after ASO treatment (*n* = 4). *Actb* as the housekeeping gene. **G** IB for cleaved caspase-3 in the cortex and spinal cord of mice at 6 WOD (*n* = 4). Approximate molecular weight markers (kDa) are shown, and GAPDH is used as loading control. **H** Quantification of IB for cleaved caspase-3 (17 kDa) in the cortex and spinal cord of treated mice. Mean ± SEM. $^{*}p < 0.05$, $^{**}p < 0.01$ and $^{***}p < 0.001$.

important for astrocytic physiological function and reactivity, we examined levels of two representative astrocytic genes. The astrocytic solute carrier family 1 member 2 gene *Slc1a2/Glt1* that encodes glutamate transporter GLT1/EAAT2 plays key roles in glutamate reuptake and modulation of homeostatic brain function, and is deficient in ALS [40]. The pan-reactive astrocytic gene *Serpina3n* encodes the serine protease inhibitor that is upregulated during neurodegeneration [36]. We detected a significant decrease of the *Slc1a2/Glt1* mRNAs in the cortex (Fig. 5G) and spinal cord (Fig. 5H) of rNLS8 mice (rNLS-Sal) compared to the control mice (Ctrl-Sal). However, there were no significant differences in the *Slc1a2/Glt1* mRNAs of rNLS-ASO mice relative to the rNLS-Sal group in the cortex or spinal cord. Similarly, rNLS8 mice (rNLS-Sal) displayed dramatic upregulation of *Serpina3n* in the spinal cord compared to Ctrl-Sal mice (Fig. 5H), although *Serpina3n* mRNAs was not significantly different in the cortex between Ctrl-Sal and rNLS-Sal mice (Fig. 5G). Nevertheless, knockdown of *Chop* did not affect *Serpina3n* mRNAs in treated mice (rNLS-ASO) compared to the rNLS-Sal group. Overall, these results not only confirmed previous reported astrogliosis in rNLS8

mice at the mid-disease stage [19] but also revealed dramatic dysregulation of disease-related astrocytic genes, suggesting disruption of astrocytic function may contribute to neurodegeneration in this model. Nevertheless, we did not identify any evidence for amelioration of disease-related astrogliosis or astrocytic gene expression alterations upon knockdown of *Chop* in rNLS8 mice.

DISCUSSION
Here, we aimed to determine which cellular stress pathways contribute to disease onset and progression in ALS, using a well-characterized mouse model of cytoplasmic TDP-43 proteinopathy. Our data identified early dysregulation of multiple genes in several signaling pathways in the cortex of pre-onset rNLS8 mice, including *Atf4, Chop, Bid, Gadd45g*, and *Trp53*, extending throughout disease progression (summarized in Fig. 6A). Most notably, we identified early activation of the ISR and alterations in apoptosis pathways even in rNLS8 mice prior to onset of motor phenotypes and continuing through early disease stages, leading
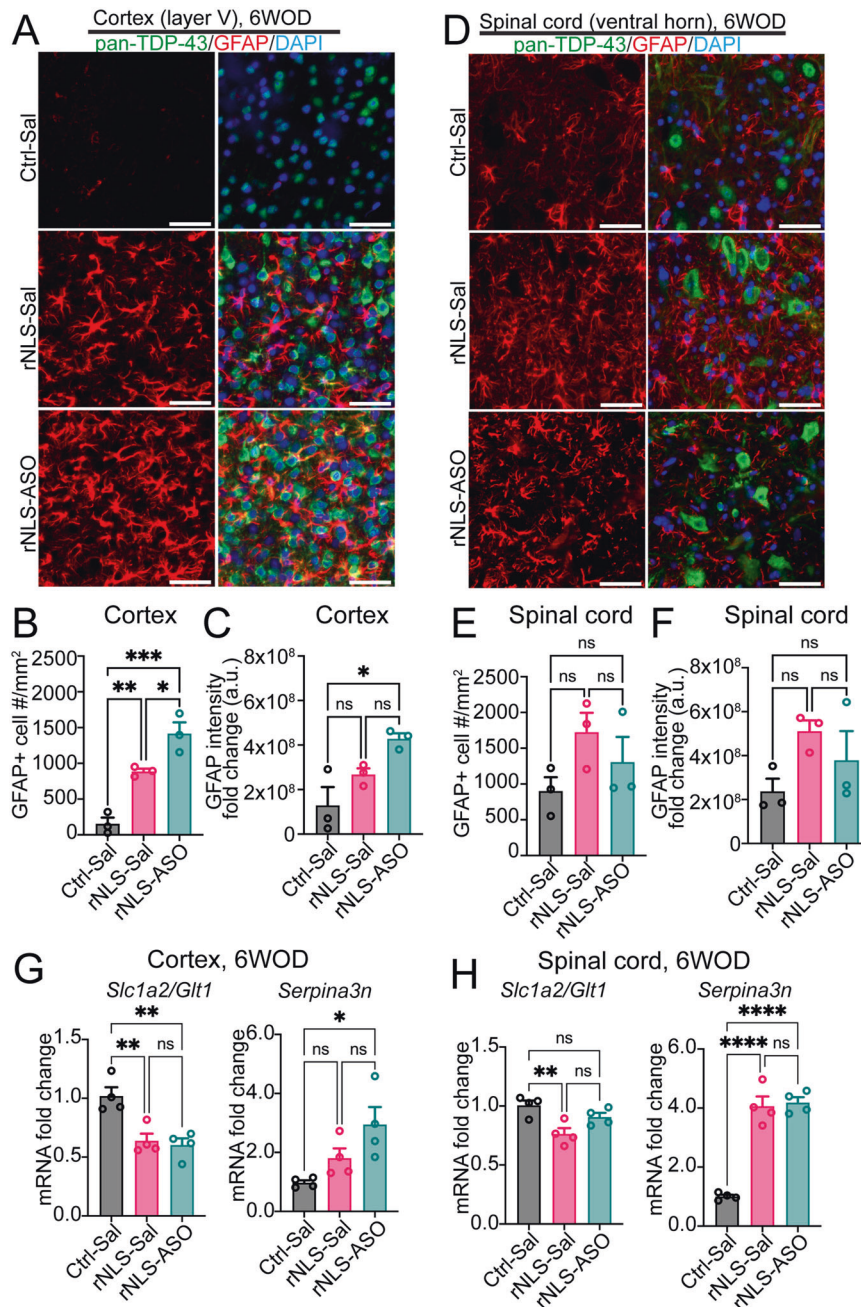
Fig. 5 rNLS8 mice develop reactive astrogliosis and altered astrocytic gene expression, which are not ameliorated by knockdown of *Chop*. Representative IF images for pan-TDP-43 (human+mouse) (green), reactive-astrocytic marker GFAP (red), and the nuclear marker DAPI (blue) in the layer V of cortex (**A**) or the ventral horn of spinal cord (**D**) of mice at 6 weeks off Dox (WOD). Scale bars represent 50 μm. Cell counting for GFAP positively labeled astrocytes in the cortex (**B**) and spinal cord (**E**) of treated mice ($n = 3$). Quantification of IF for GFAP intensity in the cortex (**C**) and spinal cord (**F**) of treated mice at 6 WOD ($n = 3$). qPCR analysis of astrocytic gene expression in the cortex (**G**) and spinal cord (**H**) of *Chop* ASO-treated mice at 6 WOD ($n = 4$). Data are normalised to *Actb* as the housekeeping gene. Mean ± SEM. $^{*}p < 0.05$, $^{**}p < 0.01$, $^{***}p < 0.001$ and $^{****}p < 0.0001$.

to later activation of caspase-3 (Fig. 6B). However, suppression of *Chop*, a key activator of the ISR, beginning prior to induction of *hTDP-43^{ΔNLS}* expression, did not ameliorate disease pathology, onset, or progression in rNLS8 mice. Together, these studies demonstrate that cellular stress pathways, possibly including early anti-apoptotic signaling, are activated prior to disease onset and may contribute to neurodegeneration in rNLS8 mice. However, suppression of *Chop* throughout disease is not sufficient to prevent a switch to pro-apoptotic signaling associated with disease progression.

In contrast to healthy neurons with tightly controlled protein synthesis, folding and degradation, in disease protein aggregation triggers the ISR which can ultimately lead to neuronal death [11, 12]. TDP-43 pathology is associated with activation of ISR in both neurons and non-neuron cells in nervous system post-mortem tissues of people who have died with ALS or FTD [41], with increased CHOP levels identified in multiple types of cells in the postmortem tissues of human ALS [17] as well as in cell and mouse models for ALS and FTD [15, 20, 42, 43]. Here in this study, the IF results demonstrate CHOP protein primarily in *hTDP-43^{ΔNLS}*-
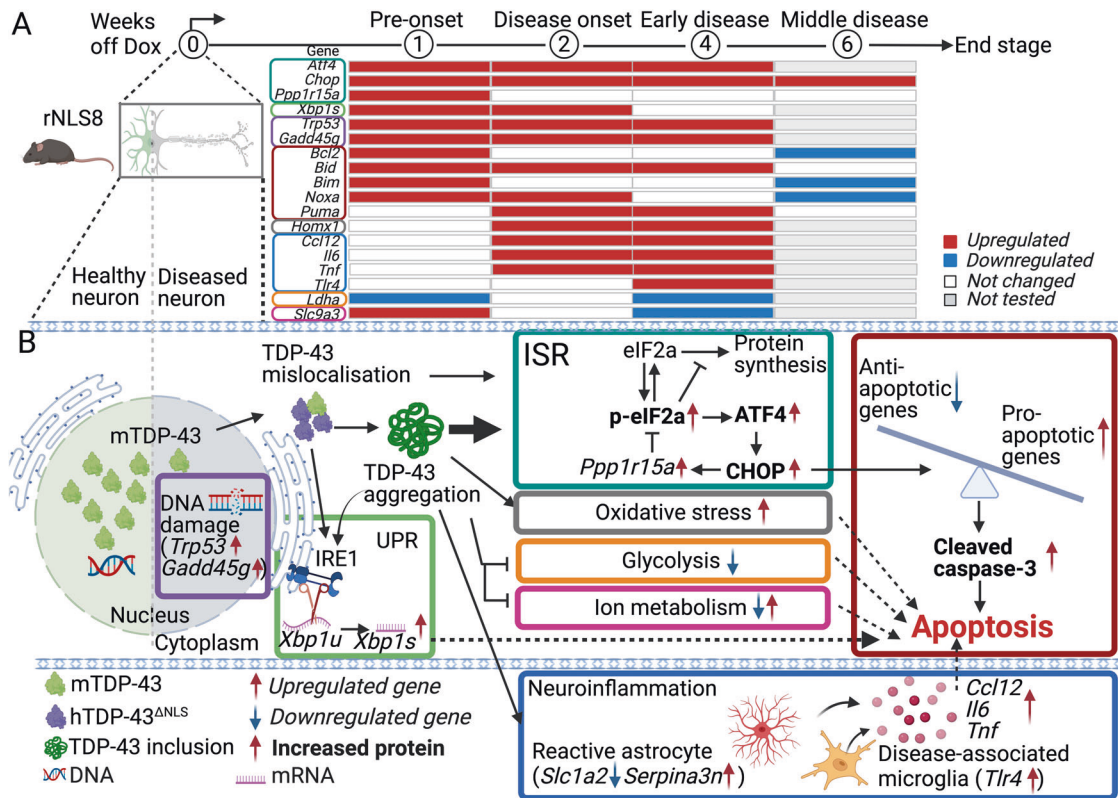
Fig. 6 **TDP-43 pathology causes early activation of the ISR and apoptosis signaling in rNLS8 mice. A** Summary of gene expression changes in the cortex of rNLS8 mice over time. **B** Mechanism schema. TDP-43 mislocalisation induces early activation of multiple cell stress signaling pathways in the cortex of rNLS8 mice even before disease onset, such as the ISR, UPR, DNA damage response, and apoptosis. Notably, the prolonged activation of these cell stress pathways caused by TDP-43 pathology, in particular the ISR, continues through early-disease stages where rNLS8 mice displayed dramatic elevation of p-eIF2α and ATF4 protein, and impairment of cellular metabolism. Dysregulation of stress pathways leads to reduction of anti-apoptotic *Bcl2*, continued increased expression of pro-apoptotic genes (*Bid, Bim, Noxa,* and *Puma*), and increases of cleaved caspase-3 and astrogliosis, likely contributing to neurodegeneration in rNLS8 mice.

positive neurons, although CHOP was also detected in some surrounding non-neuronal cells in rNLS mice. This suggests potential involvement of both cell-autonomous as well as non-cell-autonomous mechanisms in ISR activation in disease. Interestingly, in vivo, TDP-43 pathology results in global protein translation inhibition, which is the main effect of the ISR [44]. Moreover, in cell culture, disease-associated mutant TDP-43 proteins trigger ISR activation and elevation of downstream gene expression including *Chop*, involving an amplifying cell stress response potentially leading to cell death [15]. Indeed, future experiments are required to assess the effects of modulation of other ISR genes such as *Atf4*, which has broader downstream effects [11, 12] and may be involved in the clearance of TDP-43 inclusions via autophagy [45]. Furthermore, *CHOP* was recently identified as one of the top upregulated genes in a human neuronal model of TDP-43 pathology, and was shown to be a direct target of TDP-43-mediated gene expression with increased *CHOP* levels in neurons with depleted nuclear TDP-43 in human FTLD-TDP-derived samples [46]. In addition, mice expressing ALS-associated mutant SOD1 [43, 47] or ALS and FTD-associated FUS [48] also display activation of ISR and/or impairment of ongoing protein synthesis, including upregulation of *Chop* [49]. The ISR is also activated in neurons expressing expanded *C9orf72* hexanucleotide repeats, and is similarly seen in the cortices of people who have died with *C9orf72*-linked ALS and FTD [50]. Together, these studies indicate that ISR activation, and *Chop* in particular, is involved broadly in disease, although it remains unclear whether these pathways may be amenable to therapeutic targeting in TDP-43-related disease. Our data show that knockdown of *Chop* using ASO decreased *Chop* expression, but had no impact on motor

deficits or overall TDP-43 pathology. These findings are consistent with previous reports that neither genetic knockout nor ASO-mediated knockdown of *Chop* led to beneficial outcomes in the mutant SOD1^{G93A} mouse model of ALS [20, 51] or rTg4510 mice for Alzheimer's disease [52]. Nevertheless, we did detect a slight albeit statistically significant decrease of insoluble TDP-43 CTFs in ASO-treated rNLS8 mice. Indeed, previous work has suggested that TDP-43 fragmentation may occur through activation of caspases such as caspase-3, a transcriptional target of CHOP [53, 54]. However, although TDP-43 CTFs are a pathological hallmark in the brains of people with ALS or FTD, current evidence suggests that TDP-43 CTFs may not act as a primary driver of disease pathogenesis [54]. Therefore, the disease relevance of a small change in TDP-43 CTFs in ASO-treated rNLS8 mice in our study remains unclear. Future cell culture experiments to address the biochemical alterations caused by CHOP ablation in neurons and the effects of decreased CHOP levels on TDP-43 pathology may be needed to reveal the mechanisms involved in these processes.

Prolonged ISR activation induces apoptosis via cell death downstream of the intrinsic pathway that is regulated by BCL2 family members (BIM, NOXA, PUMA), and the extrinsic pathway (BID) that can be triggered by various cell death signals [10]. Notably, our results revealed that induction of hTDP-43^{ΔNLS} expression rapidly induced both anti-apoptotic (*Bcl2*) and pro-apoptotic genes (*Bim, Bid, Noxa*) in rNLS8 mice even before disease onset. In contrast, from disease onset, *Bcl2* mRNA in rNLS8 mice returned to the level similar to the control mice, coinciding with elevation of pro-apoptotic *Bid, Noxa,* and *Puma* mRNAs in rNLS8 mice, suggesting a switch from pro-survival to pro-death

signalling over time. Importantly, our findings revealed that activation of these pro-apoptotic genes occurred differentially over the disease course (summarized in Fig. 6). For example, *Bim* mRNA was increased only prior to disease onset, in line with the previous report that *Bim* gene can be induced by overexpression of TDP-43 in neurons [42]. In contrast, p53-mediated transcription of *Noxa* and *Puma* was increased in rNLS8 mice during early disease stages, consistent with our data showing upregulation of *Trp53* and *Gadd45g*. Notably, *Bid*, a gene that can be induced by a variety of upstream signals from the ISR, DNA damage, oxidative stress, and death receptors (for example, TNF and its receptor), was upregulated prior to disease onset and into early disease stages. This differential regulation of apoptotic genes indicates that multiple stress signaling pathways may co-contribute to and even enhance pro-apoptotic signaling in rNLS8 mice at different disease stages. Moreover, we speculate that significant neuron loss occurs in the motor cortex of rNLS8 mice by 6 weeks off Dox, which may partly account for the late decrease of *Bcl2, Bim*, and *Noxa* expression in rNLS8 mice, consistent with previous findings that show decreases of *Bcl2* mRNA in postmortem tissues in ALS and other human neurodegenerative diseases [35]. Importantly, rNLS8 mice displayed elevation of pro-apoptotic executioner caspase-3 at the mid-stage of disease, providing direct evidence that supports the previous findings of increased caspase-3 in brain and spinal cord autopsy tissues of people with ALS and FTD [54]. Overall, our data, therefore, supports the hypothesis that TDP-43 pathology induces apoptosis contributing to neurodegeneration, but reveals complex regulation between pro-survival and pro-death signaling that begins early in the disease course. Thus, targeting apoptosis may be a beneficial therapeutic strategy for treatment of ALS and FTD. Notably, we did not detect any changes in expression of necroptosis genes *Ripk1* and *Ripk3* at 2 or 4 weeks off Dox in rNLS8 mice, despite the detected alterations of apoptosis signalling even at these early timepoints, aligning with recent work suggesting that necroptosis is not a primary driver of neurodegeneration in ALS and FTD [55].

Our results also demonstrated dramatic astrogliosis in the cortex and spinal cord of rNLS8 mice, with significant upregulation of pan-reactive astrocytic marker *Serpina3n* in rNLS-ASO mice, which can be induced upon neuronal damage and contributes to neuroinflammation [36, 37]. Our finding is consistent with previous studies showing upregulation of *Serpina3n* in a conditional TDP-43 knockout mouse model for FTD [56], suggesting that the loss of endogenous nuclear TDP-43 in neurons of the rNLS8 mice [19] may account for this phenotype. Notably, our results also indicated the downregulation of the *Slc1a2* gene encoding glutamate transporter GLT1 in rNLS8 mice. This is in line with the previous observation that GLT1 expression is selectively decreased in astrocytes of ALS postmortem tissues [40] and also in TDP-43-associated FTD cases [57]. Hence, our results further support the hypothesis that disease-associated astrocyte reactivity and deficiency of astrocytic reuptake of glutamate at the synaptic cleft contribute to neurotoxicity in ALS and FTD. Interestingly, suppression of *Chop* via ASO slightly increased the number of reactive astrocytes, potentially supporting the previous findings that CHOP is involved in astrocyte survival [58] or astrocyte reactivation [39] under stress conditions.

In addition to ISR, other biological processes also appear active early in the rNLS8 mice, such as DNA damage response, UPR and dysfunction in cellular metabolic functions. Our data revealed dramatic elevation of *Trp53* and *Gadd45g* genes as early as 1 week off Dox and continued to early disease stages. Previous research showed depletion of TDP-43 or ALS-linked mutant TDP-43 induces DNA damage and consequently p53-dependent apoptosis of motor neurons [59, 60], while GADD45G acts as a stress sensor for p53-mediated apoptosis [61, 62]. Moreover, it is proposed that oxidative stress is a pathogenic mechanism in disease, in parallel with or downstream of ISR [4, 6]. Our results reveal elevation of the oxidative stress-responsive gene *Homx1* in the cortex of rNLS8 mice from the 2-week time point, in line with evidence from the motor cortex of ALS or FTD-linked mutant TDP-43 transgenic mice [6, 63, 64] and in the lumbar spinal cord of SOD1^{G93A} mice for ALS [65]. However, most oxidative stress genes remained unchanged in our study, suggesting that further studies are required to identify the roles of oxidative stress genes in TDP-43-related disease. Additionally, we detected significant increases of the spliced (active) form of *Xbp1*, a key component of the UPR mediated by activation of IRE1, in rNLS8 mice at 1 and 2 weeks off Dox. These results indicate involvement of early activation of UPR signaling in rNLS8 mice in response to accumulation of TDP-43 pathology, in addition to the ISR. Further, our data demonstrate early deficiency of cellular metabolism in rNLS8 mice at early disease stage (4 weeks off Dox). LDHA, encoded by the *Ldha* gene, is specifically expressed in cortical neurons (including Layer V neurons) in human and rodent brains, and plays a vital role in neuronal health, with knockdown of *Ldha* inducing intrinsic apoptotic signalling [66–68]. This suggests loss of LDHA as a mechanism by which apoptosis may be triggered in rNLS8 mice. Since many of these pathways are also regulated at translational and post-translational levels, it is worth further investigation using high-throughput protein screening, for instance, quantitative proteomics [69], to characterise the interplay among pathways involved in ALS and FTD.

Of relevance for therapeutic development, ASOs have become an increasingly promising class of drugs to target conventionally undruggable molecules or pathways in a broad range of human neurological and psychiatric diseases. For instance, the FDA-approved Nusinersen targeting SMN2 to treat spinal muscular atrophy has shown remarkable efficacy in the clinic [70]. Recently, there have been newly developed ASO drugs for ALS and FTD in clinical trials, such as Tofersen to decrease SOD1 protein synthesis [71] and an ASO to inhibit translation of *C9orf72* mRNA (WVE-004, Wave Life Sciences). Moreover, preclinical trials have also been undertaken to ameliorate TDP-43 pathology via modulation of TDP-43-regulating proteins such as *Ataxin-2* [53, 72], which are now in Phase I clinical trials (ClinicalTrials.gov, Identifier# NCT04494256). Further identification of disease-relevant targets that are able to protect against neurodegeneration caused by TDP-43 dysfunction offers hope for development of additional improved therapeutics, potentially including antisense approaches, for ALS and FTD [73].

Limitations
Among the limitations of our work, we analysed a single timepoint of administration of the *Chop* ASO, namely two weeks prior to the removal of Dox from rNLS8 mice. This allowed us to assess the effects of *Chop* suppression from before induction of hTDP-43^{ΔNLS} expression and throughout the entirety of the study. Nevertheless, short-term activation of ISR may actually be protective for cells under acute cellular stress conditions [11, 12, 16], and so it is possible that the activation of *Chop* in rNLS8 mice is a beneficial response, at least early in the disease course. Indeed, our findings of shifts in activation or inhibition of different signalling pathways prior to onset and throughout disease indicate that the effects of ISR activation may be modulated by other contributing factors, such as changes in apoptosis signalling, at different disease points. Knockdown of *Chop* from the beginning of induction of hTDP-43^{ΔNLS} may have thereby ablated any neuroprotective effects of an initial ISR activation in neurons. Therefore, future studies could determine whether *Chop* suppression beginning only later in the disease course is beneficial in extending survival. Indeed, in this study we did not examine whether knockdown of *Chop* can modify the disease phenotypes or lifespan of rNLS8 mice beyond 6 weeks off Dox, which may be necessary to identify any beneficial longer-term effects. Furthermore, recent work has highlighted the importance of the level of cellular stress for effective responses to small molecule modulators of the ISR. For

example, the small molecular ISRIB, which overcomes eIF2a phosphorylation-mediated inhibition of translation by stimulating eIF2B activity, effectively rescues protein translation inhibition under conditions of acute viral infection with low levels of p-eIF2a but is ineffective in chronic infection with high levels of p-eIF2a present [74]. These results suggest that a critical threshold of ISR activation exists in disease conditions above which normally protective therapeutic approaches become ineffective [74]. Additional studies are also required to investigate changes at a single-cell level. Lastly, ISR activation is also involved in glial activation [39]. It will therefore be important to further investigate using cell-specific approaches the effects of ISR activation on hTDP-43^ΔNLS-expressing neurons as well as surrounding glial cells, in particular reactive astrocytes [75] and disease-associated microglia [76] that are involved in disease development of ALS and FTD. Regardless, our work also highlights other likely mediators of neurotoxicity which may be more promising targets for further development, including a switch between the balance or anti- and pro-apoptotic signalling. Further work is required to investigate therapeutically relevant targets and to define the timing of therapeutic intervention to successfully ameliorate disease.

CONCLUSION

Taken altogether, we identified early activation of several distinct cellular stress pathways, notably the ISR and pro-apoptotic signalling, in the cortex of rNLS8 mice even prior to disease onset. These pathways are essential for neuronal survival-and-death decisions, indicating that the biological pathway towards neurodegeneration begins very early after accumulation of cytoplasmic TDP-43 in disease. Our data revealed that cytoplasmic TDP-43 accumulation induces pro-apoptotic caspase-3 in parallel with decreases of anti-apoptotic *Bcl2* in the central nervous system of TDP-43 mice. We conclude that multiple cellular stress pathways are active early in rNLS8 mice, notably the pro-apoptotic signalling that is activated even prior to disease onset, which likely trigger eventual motor neuron death via apoptosis following loss of competing anti-apoptotic signals. Although knockdown of the key ISR mediator *Chop* had no effect on motor deficits and did not ameliorate overall TDP-43 pathology in rNLS8 mice, our findings indicate that targeting of cell stress and death signalling may be a potential promising avenue for treatment of TDP-43-associated ALS and FTD.

REFERENCES

1. Neumann M, Sampathu DM, Kwong LK, Truax AC, Micsenyi MC, Chou TT, et al. Ubiquitinated TDP-43 in frontotemporal lobar degeneration and amyotrophic lateral sclerosis. Science. 2006;314:130–3.
2. Ling SC, Polymenidou M, Cleveland DW. Converging Mechanisms in ALS and FTD: Disrupted RNA and Protein Homeostasis. Neuron. 2013;79:416–38.
3. Tziortzouda P, Van Den Bosch L, Hirth F. Triad of TDP43 control in neurodegeneration: autoregulation, localization and aggregation. Nat Rev Neurosci. 2021;22:197–208.
4. Prasad A, Bharathi V, Sivalingam V, Girdhar A, Patel BK. Molecular Mechanisms of TDP-43 Misfolding and Pathology in Amyotrophic Lateral Sclerosis. Front Mol Neurosci. 2019;12:25.
5. Keating SS, San Gil R, Swanson MEV, Scotter EL, Walker AK. TDP-43 pathology: from noxious assembly to therapeutic removal. Prog Neurobiol. 2022;211:102229.
6. Ilieva EV, Ayala V, Jove M, Dalfo E, Cacabelos D, Povedano M, et al. Oxidative and endoplasmic reticulum stress interplay in sporadic amyotrophic lateral sclerosis. Brain. 2007;130:3111–23.
7. Charif SE, Vassallu MF, Salvanal L, Igaz LM. Protein synthesis modulation as a therapeutic approach for amyotrophic lateral sclerosis and frontotemporal dementia. Neural Regen Res. 2022;17:1423–30.
8. Liu J, Wang F. Role of Neuroinflammation in Amyotrophic Lateral Sclerosis: Cellular Mechanisms and Therapeutic Implications. Front Immunol. 2017;8:1005.
9. Philips T, Robberecht W. Neuroinflammation in amyotrophic lateral sclerosis: role of glial activation in motor neuron disease. Lancet Neurol. 2011;10:253–63.
10. Moujalled D, Strasser A, Liddell JR. Molecular mechanisms of cell death in neurological diseases. Cell Death Differ. 2021;28:2029–44.
11. Costa-Mattioli M, Walter P. The integrated stress response: From mechanism to disease. Science. 2020;368:6489.
12. Walter P, Ron D. The unfolded protein response: from stress pathway to homeostatic regulation. Science. 2011;334:1081–6.
13. Hu H, Tian M, Ding C, Yu S. The C/EBP Homologous Protein (CHOP) Transcription Factor Functions in Endoplasmic Reticulum Stress-Induced Apoptosis and Microbial Infection. Front Immunol. 2018;9:3083.
14. Hicks DA, Cross LL, Williamson R, Rattray M. Endoplasmic Reticulum Stress Signalling Induces Casein Kinase 1-Dependent Formation of Cytosolic TDP-43 Inclusions in Motor Neuron-Like Cells. Neurochem Res. 2020;45:1354–64.
15. Walker AK, Soo KY, Sundaramoorthy V, Parakh S, Ma Y, Farg MA, et al. ALS-associated TDP-43 induces endoplasmic reticulum stress, which drives cytoplasmic TDP-43 accumulation and stress granule formation. PLoS One. 2013;8:e81170.
16. de Mena L, Lopez-Scarim J, Rincon-Limas DE. TDP-43 and ER Stress in Neurodegeneration: Friends or Foes? Front Mol Neurosci. 2021;14:772226.
17. Ito Y, Yamada M, Tanaka H, Aida K, Tsuruma K, Shimazawa M, et al. Involvement of CHOP, an ER-stress apoptotic mediator, in both human sporadic ALS and ALS model mice. Neurobiol Dis. 2009;36:470–6.
18. Wright AL, Della Gatta PA, Le S, Berning BA, Mehta P, Jacobs KR, et al. Riluzole does not ameliorate disease caused by cytoplasmic TDP-43 in a mouse model of amyotrophic lateral sclerosis. Eur J Neurosci. 2021;54:6237–55.
19. Walker AK, Spiller KJ, Ge G, Zheng A, Xu Y, Zhou M, et al. Functional recovery in new mouse models of ALS/FTLD after clearance of pathological cytoplasmic TDP-43. Acta Neuropathol. 2015;130:643–60.
20. Ghadge GD, Sonobe Y, Camarena A, Drigotas C, Rigo F, Ling KK, et al. Knockdown of GADD34 in neonatal mutant SOD1 mice ameliorates ALS. Neurobiol Dis. 2020;136:104702.
21. Zamani A, Walker AK, Rollo B, Ayers KL, Farah R, O'Brien TJ, et al. Impaired glymphatic function in the early stages of disease in a TDP-43 mouse model of amyotrophic lateral sclerosis. Transl Neurodegener. 2022;11:17.
22. Swayze EE, Siwkowski AM, Wancewicz EV, Migawa MT, Wyrzykiewicz TK, Hung G, et al. Antisense oligonucleotides containing locked nucleic acid improve potency but cause significant hepatotoxicity in animals. Nucl Acids Res. 2007;35:687–700.
23. Paxinos G, Franklin KBJ, Ebscohost. Paxinos and Franklin's The mouse brain in stereotaxic coordinates. Fifth edition. edn. London: Academic Press, an imprint of Elsevier; 2019.
24. Staats KA, Schonefeldt S, Van Rillaer M, Van Hoecke A, Van Damme P, Robberecht W, et al. Beta-2 microglobulin is important for disease progression in a murine model for amyotrophic lateral sclerosis. Front Cellular Neurosci. 2013;7:249.
25. Zhou Y, Zhou B, Pache L, Chang M, Khodabakhshi AH, Tanaseichuk O, et al. Metascape provides a biologist-oriented resource for the analysis of systems-level datasets. Nat Commun. 2019;10:1523.
26. Bader GD, Hogue CW. An automated method for finding molecular complexes in large protein interaction networks. BMC Bioinforma. 2003;4:2.
27. Heberle H, Meirelles GV, da Silva FR, Telles GP, Minghim R. InteractiVenn: a web-based tool for the analysis of sets through Venn diagrams. Bmc Bioinformatics. 2015;16:169.
28. Livak KJ, Schmittgen TD. Analysis of relative gene expression data using real-time quantitative PCR and the 2(-Delta Delta C(T)) Method. Methods. 2001;25:402–8.
29. Luan W, Hammond LA, Vuillermot S, Meyer U, Eyles DW. Maternal Vitamin D Prevents Abnormal Dopaminergic Development and Function in a Mouse Model of Prenatal Immune Activation. Sci Rep. 2018;8:9741.
30. Ayala YM, De Conti L, Avendano-Vazquez SE, Dhir A, Romano M, D'Ambrogio A, et al. TDP-43 regulates its mRNA levels through a negative feedback loop. EMBO J. 2011;30:277–88.
31. Sephton CF, Cenik C, Kucukural A, Dammer EB, Cenik B, Han Y, et al. Identification of neuronal RNA targets of TDP-43-containing ribonucleoprotein complexes. J Biol Chem. 2011;286:1204–15.
32. Puthalakath H, O'Reilly LA, Gunn P, Lee L, Kelly PN, Huntington ND, et al. ER stress triggers apoptosis by activating BH3-only protein Bim. Cell. 2007;129:1337–49.
33. Yang Y, Liu L, Naik I, Braunstein Z, Zhong J, Ren B. Transcription Factor C/EBP Homologous Protein in Health and Diseases. Front Immunol. 2017;8:1612.
34. Xu L, Bi Y, Xu Y, Wu Y, Du X, Mou Y, et al. Suppression of CHOP Reduces Neuronal Apoptosis and Rescues Cognitive Impairment Induced by Intermittent Hypoxia by Inhibiting Bax and Bak Activation. Neural Plast. 2021;2021:4090441.
35. Erekat NS. Apoptosis and its therapeutic implications in neurodegenerative diseases. Clin Anat. 2022;35:65–78.
36. Wheeler MA, Jaronen M, Covacu R, Zandee SEJ, Scalisi G, Rothhammer V, et al. Environmental Control of Astrocyte Pathogenic Activities in CNS Inflammation. Cell. 2019;176:581–96.e518.
37. Schiffer D, Fiano V. Astrogliosis in ALS: possible interpretations according to pathogenetic hypotheses. Amyotroph Lateral Scler Other Mot Neuron Disord. 2004;5:22–25.
38. Yamanaka K, Komine O. The multi-dimensional roles of astrocytes in ALS. Neurosci Res. 2018;126:31–38.

39. Sims SG, Cisney RN, Lipscomb MM, Meares GP. The role of endoplasmic reticulum stress in astrocytes. Glia. 2022;70:5–19.

40. Rothstein JD, Van Kammen M, Levey AI, Martin LJ, Kuncl RW. Selective loss of glial glutamate transporter GLT-1 in amyotrophic lateral sclerosis. Ann Neurol. 1995;38:73–84.

41. Tam OH, Rozhkov NV, Shaw R, Kim D, Hubbard I, Fennessey S, et al. Postmortem Cortex Samples Identify Distinct Molecular Subtypes of ALS: Retrotransposon Activation, Oxidative Stress, and Activated Glia. Cell Rep. 2019;29:1164–77.

42. Suzuki H, Matsuoka M. TDP-43 toxicity is mediated by the unfolded protein response-unrelated induction of C/EBP homologous protein expression. J Neurosci Res. 2012;90:641–7.

43. Wang L, Popko B, Roos RP. An enhanced integrated stress response ameliorates mutant SOD1-induced ALS. Hum Mol Genet. 2014;23:2629–38.

44. Charif SE, Luchelli L, Vila A, Blaustein M, Igaz LM. Cytoplasmic Expression of the ALS/FTD-Related Protein TDP-43 Decreases Global Translation Both in vitro and in vivo. Front Cell Neurosci. 2020;14:594561.

45. Chu YP, Jin LW, Wang LC, Ho PC, Wei WY, Tsai KJ. Transthyretin attenuates TDP-43 proteinopathy by autophagy activation via ATF4 in FTLD-TDP. Brain. 2023;00:1-18.

46. Hruska-Plochan M, Betz KM, Ronchi S, Wiersma VI, Maniecka Z, Hock E-M, et al. Human neural networks with sparse TDP-43 pathology reveal NPTX2 mis-regulation in ALS/FTLD. bioRxiv https://doi.org/10.1101/2021.12.08.471089.

47. Kikuchi H, Almer G, Yamashita S, Guegan C, Nagai M, Xu Z, et al. Spinal cord endoplasmic reticulum stress associated with a microsomal accumulation of mutant superoxide dismutase-1 in an ALS model. Proc Natl Acad Sci. 2006;103:6025–30.

48. Lopez-Erauskin J, Tadokoro T, Baughn MW, Myers B, McAlonis-Downes M, Chillon-Marinas C, et al. ALS/FTD-Linked Mutation in FUS Suppresses Intra-axonal Protein Synthesis and Drives Disease Without Nuclear Loss-of-Function of FUS. Neuron. 2018;100:816–30.e817.

49. Shelkovnikova TA, An H, Skelt L, Tregoning JS, Humphreys IR, Buchman VL. Antiviral Immune Response as a Trigger of FUS Proteinopathy in Amyotrophic Lateral Sclerosis. Cell Rep. 2019;29:4496–508.e4494.

50. Parameswaran J, Zhang N, Tilahun K, Pant DC, Chilukuri G, Asress S, et al. Anti-sense, but not sense, repeat expanded RNAs activate PKR/eIF2α-dependent integrated stress response in C9orf72 FTD/ALS. bioRxiv https://doi.org/10.1101/2022.06.06.495030.

51. Dzhashiashvili Y, Monckton CP, Shah HS, Kunjamma RB, Popko B. The UPR-PERK pathway is not a promising therapeutic target for mutant SOD1-induced ALS. Neurobiol Dis. 2019;127:527–44.

52. Criado-Marrero M, Blazier DM, Gould LA, Gebru NT, Ospina SR, Armendariz DS, et al. Evidence against a contribution of the CCAAT-enhancer binding protein homologous protein (CHOP) in mediating neurotoxicity in rTg4510 mice. Sci Rep. 2022;12:7372.

53. Hart MP, Gitler AD. ALS-associated ataxin 2 polyQ expansions enhance stress-induced caspase 3 activation and increase TDP-43 pathological modifications. J Neurosci. 2012;32:9133–42.

54. Berning BA, Walker AK. The Pathobiology of TDP-43 C-Terminal Fragments in ALS and FTLD. Front Neurosci. 2019;13:335.

55. Wang TD, Perera ND, Chiam MDF, Cuic B, Wanniarachchillage N, Tomas D, et al. Necroptosis is dispensable for motor neuron degeneration in a mouse model of ALS. Cell Death Differ. 2020;27:1728–39.

56. Wu LS, Cheng WC, Chen CY, Wu MC, Wang YC, Tseng YH, et al. Transcriptomopathies of pre- and post-symptomatic frontotemporal dementia-like mice with TDP-43 depletion in forebrain neurons. Acta Neuropathol Commun. 2019;7:50.

57. Tollervey JR, Curk T, Rogelj B, Briese M, Cereda M, Kayikci M, et al. Characterizing the RNA targets and position-dependent splicing regulation by TDP-43. Nat Neurosci. 2011;14:452–U180.

58. Benavides A, Pastor D, Santos P, Tranque P, Calvo S. CHOP plays a pivotal role in the astrocyte death induced by oxygen and glucose deprivation. Glia. 2005;52:261–75.

59. Mitra J, Guerrero EN, Hegde PM, Liachko NF, Wang H, Vasquez V, et al. Motor neuron disease-associated loss of nuclear TDP-43 is linked to DNA double-strand break repair defects. Proc Natl Acad Sci. 2019;116:4696–705.

60. Giannini M, Bayona-Feliu A, Sproviero D, Barroso SI, Cereda C, Aguilera A. TDP-43 mutations link Amyotrophic Lateral Sclerosis with R-loop homeostasis and R loop-mediated DNA damage. PLoS Genet. 2020;16:e1009260.

61. Maor-Nof M, Shipony Z, Lopez-Gonzalez R, Nakayama L, Zhang YJ, Couthouis J, et al. p53 is a central regulator driving neurodegeneration caused by C9orf72 poly(PR). Cell. 2021;184:689.

62. Salvador JM, Brown-Clay JD, Fornace AJ Jr. Gadd45 in stress signaling, cell cycle control, and apoptosis. Adv Exp Med Biol. 2013;793:1–19.

63. Zuo X, Zhou J, Li Y, Wu K, Chen Z, Luo Z, et al. TDP-43 aggregation induced by oxidative stress causes global mitochondrial imbalance in ALS. Nat Struct Mol Biol. 2021;28:132–42.

64. Guo Y, Wang Q, Zhang K, An T, Shi P, Li Z, et al. HO-1 induction in motor cortex and intestinal dysfunction in TDP-43 A315T transgenic mice. Brain Res. 2012;1460:88–95.

65. Dwyer BE, Lu SY, Nishimura RN. Heme oxygenase in the experimental ALS mouse. Exp Neurol. 1998;150:206–12.

66. Bittar PG, Charnay Y, Pellerin L, Bouras C, Magistretti PJ. Selective distribution of lactate dehydrogenase isoenzymes in neurons and astrocytes of human brain. J Cereb Blood Flow Metab. 1996;16:1079–89.

67. Laughton JD, Charnay Y, Belloir B, Pellerin L, Magistretti PJ, Bouras C. Differential messenger RNA distribution of lactate dehydrogenase LDH-1 and LDH-5 isoforms in the rat brain. Neuroscience. 2000;96:619–25.

68. Valvona CJ, Fillmore HL, Nunn PB, Pilkington GJ. The Regulation and Function of Lactate Dehydrogenase A: Therapeutic Potential in Brain Tumor. Brain Pathol. 2016;26:3–17.

69. Hedl TJ, San Gil R, Cheng F, Rayner SL, Davidson JM, De Luca A, et al. Proteomics Approaches for Biomarker and Drug Target Discovery in ALS and FTD. Front Neurosci. 2019;13:548.

70. Bennett CF, Kordasiewicz HB, Cleveland DW. Antisense Drugs Make Sense for Neurological Diseases. Annu Rev Pharm. 2021;61:831–52.

71. Miller T, Cudkowicz M, Shaw PJ, Andersen PM, Atassi N, Bucelli RC, et al. Phase 1-2 Trial of Antisense Oligonucleotide Tofersen for SOD1 ALS. N Engl J Med. 2020;383:109–19.

72. Becker LA, Huang B, Bieri G, Ma R, Knowles DA, Jafar-Nejad P, et al. Therapeutic reduction of ataxin-2 extends lifespan and reduces pathology in TDP-43 mice. Nature. 2017;544:367–71.

73. Boros BD, Schoch KM, Kreple CJ, Miller TM. Antisense Oligonucleotides for the Study and Treatment of ALS. Neurotherapeutics 2022;19:1145–58.

74. Rabouw HH, Langereis MA, Anand AA, Visser LJ, de Groot RJ, Walter P, et al. Small molecule ISRIB suppresses the integrated stress response within a defined window of activation. P Natl Acad Sci. 2019;116:2097–102.

75. Prater KE, Latimer CS, Jayadev S. Glial TDP-43 and TDP-43 induced glial pathology, focus on neurodegenerative proteinopathy syndromes. Glia. 2022;70:239–55.

76. Hunter M, Spiller KJ, Dominique MA, Xu H, Hunter FW, Fang TC, et al. Microglial transcriptome analysis in the rNLS8 mouse model of TDP-43 proteinopathy reveals discrete expression profiles associated with neurodegenerative progression and recovery. Acta Neuropathol Commun. 2021;9:140.

AUTHOR CONTRIBUTIONS
WL, ALW, SL, FR, PJN, KL and AKW designed research. WL, ALW, HBW, LMSM and AKW performed research. WL, ALW, HBW, SL, RSG and AKW contributed unpublished reagents/analytic tools. WL, ALW, HBW, RSG and AKW analysed data. WL, ALW, RSG and AKW wrote the paper. All authors read and approved the final manuscript.

COMPETING INTERESTS
SL was employed by Nikon Australia (Healthcare Division). KL, PJN and FR are employees of Ionis Pharmaceuticals, Inc. The other authors declare no competing interest.

ETHICAL APPROVAL
All animal procedures were conducted with approved from the Animal Ethics Committee of Macquarie University (#2016-026), and the Animal Ethics Committee of

The University of Queensland (#QBI/131/18), in accordance with the Australian Code of Practice for the Care and Use of Animals for Scientific Purposes.

ADDITIONAL INFORMATION